Article

Host Defense Peptide Piscidin and Yeast-Derived Glycolipid Exhibit Synergistic Antimicrobial Action through Concerted Interactions with Membranes

Fei Liu, Alexander I. Greenwood, Yawei Xiong, Rebecca T. Miceli, Riqiang Fu, Kyle W. Anderson, Scott A. McCallum, Mihaela Mihailescu, Richard Gross,* and Myriam L. Cotten*

Cite This: *JACS Au* 2023, 3, 3345−3365

Read Online

| ACCESS | | 📊 Metrics & More | | 📖 Article Recommendations | | 🗐 Supporting Information |

ABSTRACT: Developing new antimicrobials as alternatives to conventional antibiotics has become an urgent race to eradicate drug-resistant bacteria and to save human lives. Conventionally, antimicrobial molecules are studied independently even though they can be cosecreted *in vivo*. In this research, we investigate two classes of naturally derived antimicrobials: sophorolipid (SL) esters as modified yeast-derived glycolipid biosurfactants that feature high biocompatibility and low production cost; piscidins, which are host defense peptides (HDPs) from fish. While HDPs such as piscidins target the membrane of pathogens, and thus result in low incidence of resistance, SLs are not well understood on a mechanistic level. Here, we demonstrate that combining SL−hexyl ester (SL-HE) with subinhibitory concentration of piscidins 1 (P1) and 3 (P3) stimulates strong antimicrobial synergy, potentiating a promising therapeutic window. Permeabilization assays and biophysical studies employing circular dichroism, NMR, mass spectrometry, and X-ray diffraction are performed to investigate the mechanism underlying this powerful synergy. We reveal four key mechanistic features underlying the synergistic action: (1) P1/3 binds to SL-HE aggregates, becoming α-helical; (2) piscidin−glycolipid assemblies synergistically accumulate on membranes; (3) SL-HE used alone or bound to P1/3 associates with phospholipid bilayers where it induces defects; (4) piscidin−glycolipid complexes disrupt the bilayer structure more dramatically and differently than either compound alone, with phase separation occurring when both agents are present. Overall, dramatic enhancement in antimicrobial activity is associated with the use of two membrane-active agents, with the glycolipid playing the roles of prefolding the peptide, coordinating the delivery of both agents to bacterial surfaces, recruiting the peptide to the pathogenic membranes, and supporting membrane disruption by the peptide. Given that SLs are ubiquitously and safely used in consumer products, the SL/peptide formulation engineered and mechanistically characterized in this study could represent fertile ground to develop novel synergistic agents against drug-resistant bacteria.

KEYWORDS: antimicrobial peptides, glycolipids, synergy, minimum inhibitory concentrations, circular dichroism, solid-state NMR, surface plasmon resonance, membrane permeabilization
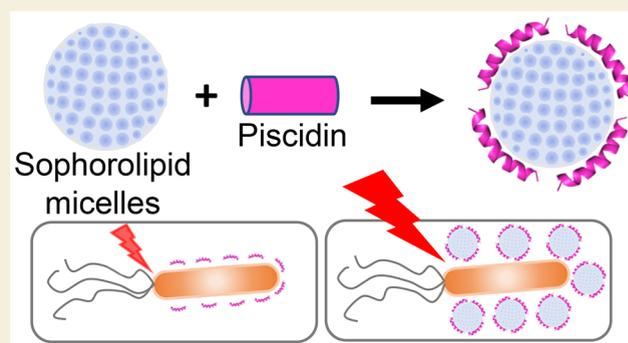
■ INTRODUCTION

In the face of proliferating strains of drug-resistant bacteria worldwide, discovering novel antibiotics has become an urgent race to save human lives.[1−5] Nature abounds with molecules with antimicrobial functions, given that this biological activity is essential to species survival. *In vivo*, antimicrobial substances are usually cosecreted to fight pathogens, leading to complementary or synergistic action.[6−14] Synergy occurs when compounds produce an effect that is greater than the sum of their individual activities. In recent years, several approaches exploiting synergistic action have been investigated to fight drug-resistant bacteria.[1,7,15,16] A particular advantage of synergistic drug formulations is that lower drug concentrations are needed to achieve potency, thereby reducing the cost, side effects, and

incidence of resistance. However, little is known about the mechanisms underlying synergistic antibacterial effects, impeding our ability to leverage such strategies for the development of novel antimicrobials. New strategies are also needed to enable the agents to simultaneously access their targets *in vivo* since this is a prerequisite to potentiating synergistic effects.

Different approaches have been explored to achieve a synergistic action between antimicrobial compounds. For instance, multidrug therapy can be used to invert the benefit associated with the selective advantage of resistance to the first drug.[1] Practically, a first drug is used to generate a set of resistant mutants that are disadvantageous when confronted with a second drug. Another approach is to combine conventional antibiotics with compounds that have a lower rate of resistance since their broad spectrum of action involves acting on vital parts of the cells that cannot be readily mutated without compromising cell survival. In particular, several host defense peptides (HDPs), which are typically broad spectrum, have been successfully combined with antibiotics.[6,10,11,16−27] However, the possibility that HDPs could be synergized with other classes of naturally occurring broad spectrum antimicrobial molecules such as glycolipids remains mostly uncharacterized. In this research, we feature the synergistic antimicrobial action of cationic and amphipathic HDPs with a glycolipid derived from yeast. The glycolipid, which is cost-effective to produce and features high biocompatibility properties, is boosted by submicromolar inhibitory concentration of peptide, enabling a lower dosage of the agent that is more costly and has a narrower therapeutic window.

HDPs have been investigated extensively due to their essential role in innate immunity and promising attributes as novel anti-infective agents against drug-resistant bacteria.[28−33] Being broad spectrum, HDPs generally eradicate pathogens by membrane disruption and/or intracellular targeting after crossing the plasma membrane.[16,32,34−41] In the Antimicrobial Peptide Database (APD), more than 3000 HDP sequences have been reported. Among those with known secondary structures, about 45% feature α-helical content.[42] A significant hurdle to developing them into potent, safe, and affordable therapeutic agents is the need to identify strategies such as sequence optimization or combination with other antimicrobials to enhance their efficacies so that the dosage and side effects can be reduced.

Piscidin 1 (P1; FFHHIFRGIVHVGKTIHRLVTG-NH$_2$) and piscidin 3 (P3; FIHHIFRGIVHAGRSIGRFLTG-NH$_2$) were first discovered in hybrid striped bass.[43,44] While they are both potent antimicrobials, including on drug-resistant bacteria, P1 generally has higher antimicrobial and hemolytic activities.[43−53] Both HDPs are differentially expressed, with P3 more present in vascularized tissues.[54] We recently showed that they have complementary modes of action: P1 has stronger membrane permeabilization activity while P3 is more effective at disrupting DNA.[46,47] Membrane activity for piscidin occurs through the formation of transient defects rather than the stable pores formed by peptide toxins.[50] DNA damage involves charge neutralization and aggregation of the nucleic acid chains as the cationic peptides neutralize negative charges on DNA.[47] Examples of other cationic and histidine-rich peptides that interact with DNA and have cell penetrating function include LAH4.[55]

Sophorolipids (SLs) are a group of antimicrobial glycolipid biosurfactants derived from the nonpathogenic fungus species *Starmerella bombicola*, through the fermentation of carbohydrates and lipids.[56,57] They possess a hydrophilic sophorose, a disaccharide of glucose units linked at β-1,2, and a hydrophobic ω-1-hydroxylated oleic acid.[58] SLs have antibacterial, anticancer, antiviral, antifungal, anti-inflammatory, spermicidal, and septic shock applications.[59] SLs can be produced by efficient fermentation processes in high volumetric yields (~200 g/L).

Natural SLs can also be easily modified through ring-opening and alkylation reactions, and several synthetically modified SLs have shown improved therapeutic biological activities.[60−64] Due to their low costs, high yields, and bioactivities, SLs can be a competitive therapeutic option for disadvantaged populations seeking medical intervention.[58,65]

Naturally produced diacetylated lactonic sophorolipid can be ring-opened by alcoholysis forming a family of sophorolipid esters.[60−64,66] Of particular interest in this work is the sophorolipid hexyl ester (SL-HE), which is displayed in Figure 1 and has a molecular weight of 707 g/mol.[62,67,68] SLs have been
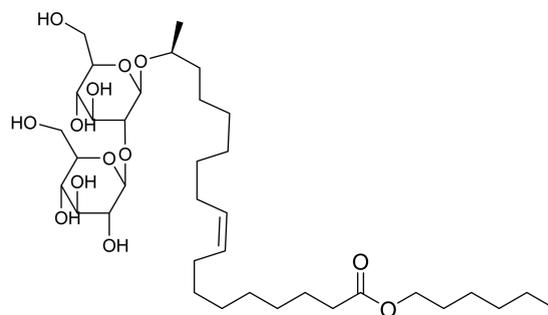
Figure 1. Glycolipid chemical structure. The sophorolipid-hexyl ester (SL-HE) used in this work is made of a glucose-derived disaccharide attached to a fatty acid via an ester bond.

extensively studied in solution. They form micelles above a critical micellar concentration (CMC) due to their amphipathic structures.[67,69] While the precise manner by which SL-esters such as SL-HE organize in micelles remains unknown, it is expected that, in aqueous media, the sugar moiety faces the aqueous solution while the acyl chains are embedded inside the micellar aggregate.[69] Their antimicrobial activity has been reported on *Bacillus cereus* (*B. cereus*), *Bacillus subtilis* (*B. subtilis*), *Staphylococcus aureus* (*S. aureus*), *Listeria innocua*, and *Escherichia coli* (*E. coli*).[64] It was noted that related SL esters can have drastically different efficacy on bacteria. For instance, the SL-butyl ester (SL-BE) has a low MIC of 12 μM on *B. cereus* and *B. subtilis*.[64] However, SL-HE was ineffective on these bacteria when tested at concentrations up to 200 μM. It has been challenging to interpret these results since few studies have investigated their mechanism of cell death and antimicrobial action (for a recent review, see ref [70]). Based on their amphiphilic character, it has been speculated that SLs could act on pathogenic cells via membrane activity, but direct evidence for this mode of action is lacking.

In this study, we hypothesized that the amphipathic structures of piscidin and SL-esters such as SL-butyl ester (SL-BE) and SL-HE promote concerted interactions with microbial membranes, thereby potentiating synergistic membrane activity and antimicrobial activity. To test this hypothesis, a combination of biological assays on *B. cereus* and biophysical studies on model membranes were performed. Remarkably, SL-HE, which is ineffective alone at >200 μM on *B. cereus*, stimulated strong synergistic antimicrobial effects when concentrations as low as 8 μM were combined with submicromolar P1/3 concentrations. Like other SL-esters, SL-HE has not been mechanistically studied previously. Here, we reveal that it is membrane active. Through biophysical studies of the SL-HE/piscidin combinations, we unveil that enhanced membrane activity and synergistic antimicrobial activity can be engineered by leveraging the ability of SL-HE to prefold piscidin, enabling

the concerted delivery of both agents to bacterial surfaces and drawing the peptide to pathogenic membranes. This novel approach to synergistic antimicrobial activity holds promise for the development of alternatives to conventional antibiotics that are prone to a high incidence of resistance.

■ MATERIALS AND METHODS

Materials, Peptide Synthesis, and Purification

The two piscidin peptides P1 (FFHHIFRGIVHVGKTIHRLVTG, MW 2571) and P3 (FIHHIFRGIVHAGRSIGRFLTG, MW 2492) were synthesized with carboxyamidated ends by solid-phase peptide synthesis at the University of Texas Southwestern Medical Center. Subsequently, they were purified by HPLC, as previously described.[45,51,71] The purified peptides were washed with dilute HCl and dialyzed to substitute chloride ions for trifluoroacetate ions, leading to 98% pure peptides, as determined by HPLC and mass spectrometry.[51] The concentrations of peptide stock solutions, reconstituted in nanopure water, were on the order of 200−300 μM, as obtained by amino acid analysis performed at the Protein Chemistry Center at Texas A&M (College Station, TX). All lipids were purchased from Avanti Polar Lipids (Alabaster, AL). SL-HE was synthesized from the natural fermentation compound lactonic sophorolipid.[62,66] Tryptic soy broth (TSB) was purchased from Becton Dickinson (Franklin Lakes, NJ) and Mueller-Hinton broth (MHB) (Sigma-Aldrich, St. Louis, MO). The reagents sodium hydroxide, Trisma hydrochloride, Trisma sodium hydroxide, sodium chloride, potassium chloride, sodium phosphate dibasic, potassium phosphate monobasic, chloroform, methanol, calcein dye, and EDTA were purchased from Sigma-Aldrich (Saint Louis, MO). The buffers 3-[(3-cholamidopropyl)-dimethylammonio]-1-propanesulfonate (CHAPS) and HEPES were obtained from Amresco (Solon, NJ) and Fisher Scientific (Hampton, NH), respectively. Nanopure water was obtained by using the Millipore Milli-Q system (Sigma-Aldrich, Saint Louis, MO).

Susceptibility Test

The minimum inhibitory concentrations (MICs) were determined using the broth dilution technique published by Clinical and Laboratory Standards Institute (CLSI).[72] Gram positive *Bacillus cereus* (ATCC 4342) bacteria were cultured in TSB for 16 h prior to being subcultured for 2.5−3 h, until they reached mid-log phase. Next, 100 μL aliquots of the subculture (2×10^5 CFU/mL) in TSB were transferred to wells from a 96-well plate before adding 100 μL of P1, P3, or SL-HE solution, which was prepared from the serial dilution of a stock made in phosphate-buffered saline (PBS). Each condition was plated in triplicates. The optical density (OD) was measured after shaking at 220 rpm and incubating for 16 h at 37 °C. The inhibition rate was calculated by using the equation $[1 - (OD_{well} - OD_{background})/(OD_{drug-free well} - OD_{background})] \times 100\%$, where the background was measured using the TSB/PBS mixture in the absence of bacteria, peptide, and SL-HE. The MIC was defined as the lowest concentration that showed ≥90% inhibition of growth compared to the control.

Synergy Test

Synergy testing was performed using the two-dimensional microbroth checkerboard method.[73] As for the susceptibility test, stock solutions of piscidin and SL were subjected to 2-fold serial dilutions. They were then distributed on a 96-well plate at concentrations of 0, 0.250, 0.500, 1.00, 2.00, 4.00, 8.00, and 16.0 μM. SL-HE was also tested at a concentration of 0.125 μM. P1 and P3 were added along columns in descending concentration. The SL was distributed similarly along rows. Each condition was plated in duplicates. As a result, each well contained a unique combination of piscidin and SL ester concentrations. To assess the possible synergy between each peptide and SL, we calculated the fractional inhibitory concentration (FIC) index using the following equation

$$FIC = (C_{piscidin}/MIC_{piscidin}) + (C_{SL}/MIC_{SL}) \quad (1)$$

where $MIC_{piscidin}$ and MIC_{SL} are the respective MICs of piscidin and SL acting alone while $C_{piscidin}$ and C_{SL} are their MICs in combination; i.e.,

their respective concentrations in the well where growth is at least 90% inhibited. Mathematically, FIC < 1 indicates synergy between compounds. However, due to the error associated with administrating the assay (e.g., serial dilution), it is more rigorous to interpret an FIC index ≤0.5 as good synergy and an FIC index of 0.5−1 as an indication of additivity.[74]

Permeabilization Assays on Bacterial Cells

The membrane activity of SL-HE and piscidin alone or in combination was obtained using a previously described protocol.[64] Briefly, we used the fluorescence probe diS-C3(5) knowing that electrically polarized cell membranes can quench it. Membrane-active substances disrupt this polarization, leading the dye to recover its fluorescence. *B. cereus* was grown to mid-log phase and diluted in fresh MHB to 2.5×10^6 CFU/mL. Next, 100 μL of this cell suspension was mixed with 50 μL of PBS containing SL-HE and piscidin, either alone or in combination. The mixture was incubated at 37 °C for 1 h. PBS served as a negative control. The assay was done in triplicates. The fluorescence was collected at 670 nm, following excitation at 622 nm using a Molecular Devices SPECTRAmax Plus 384 UV−vis High Throughput Microplate Spectrophotometer (Molecular Devices, San Jose, CA). The readings were normalized against those of the PBS negative control.

Permeabilization Assays on Synthetic Phospholipid Vesicles

The calcein-leakage assay was performed on synthetic vesicles, as previously described for piscidin.[49] Briefly, calcein-loaded large unilamellar vesicles (LUVs) were prepared using 4 μmol of total lipid (3:1 1-palmitoyl-2-oleoyl-*sn*-glycero-3-phosphocholine [POPC]/1-palmitoyl-2-oleoyl-*sn*-glycero-3-phosphoglycerol [POPG]), 3:1 POPC/POPG, in chloroform. Combinations of PC and PG have been used by our group and others to mimic the anionic surface of bacterial cells.[45,47,71,75−81] The solvent was evaporated using N_2 gas, and the sample was dried under vacuum overnight. Next, the film was hydrated with 300 μL of 80 mM calcein dye (pH = 7.4) before undergoing at least 3 freeze−thaw cycles and extrusion through a 0.1 μm polycarbonate membrane (Whatman, Florhan Park, NJ). The vesicles containing the dye were separated from free dye using a Sephadex G-50 resin column and HEPES buffer (50 mM, 100 mM NaCl, 0.3 mM EDTA, pH 7.4). Next, 180 μL of vesicles diluted to 42 μM were distributed in each well of the 96-well plate.

To prepare the SL-HE/piscidin mixture for the dye leakage assay, a small amount of SL-HE (~5 mg) was dissolved into methanol (~100 μL), sealed, and then briefly heated to facilitate dissolution. In parallel, 150 μL of either P1 or P3 was diluted to 150 μM with nanopure water. Peptides were incubated with the needed amount of SL-HE solution (~2 μL) to reach a peptide-to-sophorolipid ratio (P/SL) = 1:8. Binding was allowed to occur for 10 min. This solution was then subjected to serial dilution, so that the lipid-to-peptide molar ratio (L/P) in the wells was 2:1, 4:1, 8:1, 16:1, 32:1, 64:1, 128:1 and 256:1 upon mixing 20 μL of the peptide solutions with 180 μL of LUVs. A total phosphorus assay was performed to determine the lipid concentration LUVs (42 μM in the wells).[82] Two independent measurements were performed in triplicates. As positive and negative controls, we used 0.1% Triton-X (final concentration in the well) and nanopure water, respectively. The plate was shaken for an hour at 20 °C and cooled for 10 min before reading the fluorescence using a Bio Tek SynergyH1 plate reader (Bio Tek, Winooski, VT). Fractional dye leakage was calculated using the following equation:

$$\% \text{ leakage} = \frac{I_x - I_{0\%}}{I_{100\%} - I_{0\%}} \quad (2)$$

where I_x is the fluorescence intensity in the peptide-containing well, $I_{100\%}$ is the average intensity from the Triton-X-containing wells (100% leakage), and $I_{0\%}$ is the average intensity for wells containing the water control (0% leakage). The fractional leakage (mean of triplicates ± SD) was graphed against L/P and fitted to an adaptation of the Hill equation to yield the EC_{50} or concentration at which 50% of the vesicles are lysed.[83] The fitting was done in GraphPad Prism using least-squares regression.

Mass Spectrometry

Lipid films (~6 mg) containing a 3:1 ratio of POPC to POPG were made using solutions of POPC and POPG dissolved in chloroform. After removing the chloroform under a flow of nitrogen, the films were placed under a vacuum to dry overnight. For the P1-only sample, sufficient P1 was dissolved in water at a concentration of about 400 μM and added to the lipid film at L/P = 20:1. The volume to hydrate the lipid film was adjusted to 10 mL by adding phosphate buffer (3 mM, pH 7.4). To make a 3:1 POPC/POPG blank, the film was hydrated with 10 mL of phosphate buffer (3 mM, pH 7.4). For the sample containing P1 and SL-HE, the SL-HE dissolved in methanol was added to P1 (~1 mg) in water at P/SL = 1:8. This mixture (<1 mL) was added to the lipid film and the volume, adjusted to 10 mL using phosphate buffer (3 mM, pH 7.4). To make a sample containing the SL-HE glycolipid but no P1, the same sample was made with the exception that P1 was omitted. All hydrated lipid films were gently swirled to suspend the lipid material in the buffer and incubated overnight before being centrifuged the next day at 23 700 rpm using a Beckman centrifuge with SW40Ti rotor (Beckman, Pasadena, CA). The pellet was collected and lyophilized. Subsequently, the dry samples were dissolved in 600 μL of 1:1 water/methanol to a lipid concentration of 10 mg/mL (13 mmol/L). Prior to MS analysis, samples from pellets were diluted to ~2.5 μmol/L in 1:1 water/methanol. The samples were analyzed by electrospray ionization mass spectrometry (ESI-MS) using an Orbitrap Elite (Thermo Fisher, San Jose, CA) instrument in both positive and negative modes. Samples were directly infused into the mass spectrometer at 10 μL/min. MS results were interpreted in Xcalibur software (ThermoFisher, Waltham, MA).

Surface Plasmon Resonance

The experiments were performed following a protocol previously used for piscidin.[48] Briefly, lipid films were made using 3:1 POPC/POPG in round-bottom flasks by codissolving the two lipids in chloroform. After evaporating the solvent and drying under vacuum overnight, the films were rehydrated in working buffer (10 mM Tris pH 7.4, 100 mM NaCl) and suspended by sonication. After 3 freeze−thaw cycles, they were extruded 20 times through a 50 nm membrane (GE Healthcare, Chicago, IL) to generate small unilamellar vesicles (SUVs) and diluted 10-fold to 0.5 mM using the working buffer. The SPR experiments were carried out on a Biacore 3000 (GE Healthcare, Chicago, IL) instrument using a Biacore L1 chip (GE Healthcare, Chicago, IL) following the manufacturer's instructions. When the SUVs come in contact with the L1 chip, they form supported lipid bilayers (SLB).[84] The running buffer was 10 mM Tris pH 7.4 with 100 mM NaCl while 20 mM CHAPS was used as the regeneration solution. All solutions were freshly made, degassed, and filtered through a 0.22 μm filter (Corning, Corning, NY). At the start of each experiment, the L1 sensor chip was rinsed with 20 mM CHAPS at a flow rate of 5 μL/min for 1 min. Next, 30 μL SUVs were flowed onto the chip surface at a rate of 2 μL/min. To remove excess lipids and stabilize the baseline before applying analytes, a short pulse of 30 μL of 10 mM NaOH at a flow rate of at 50 μL/min was applied. Next, 60 μL of buffer was flowed at 30 μL/min. At this point, the SLB was ready for measurements with the analytes. P1 and P3 were serially diluted in the Tris running buffer, and SL-HE was serially diluted in PBS buffer (pH 7.4). The final solution injected as the analyte contained running buffer and PBS in a 1:1 (v/v) ratio. A total of 60 μL of analyte solution was injected at 30 μL/min over the SLB. To enable loosely bound analyte to dissociate from the SLB, flow of the running buffer alone was continued onto the chip for 5 min. All experiments were carried out at room temperature. Sensorgrams showing response units vs time (s) were graphed.

Circular Dichroism

Titrations of peptides P1 and P3 by SL-HE were followed by CD in phosphate buffer (3 mM, pH 7.4). A 1 mM solution of sophorolipid was prepared in warm phosphate buffer (~40 °C) in the presence of 10% methanol (due to the low solubility of the lipids in plain buffer). Each titration was performed at a fixed peptide concentration (25 μM) and ran in duplicates. CD spectra were recorded at 298 K on a Jasco J-815 spectrometer (Jasco Analytical Instruments, Easton, MD) over a

wavelength range of 190−260 nm by using a scan speed of 100 nm/min, a 1 nm bandwidth, and four scans. Individual samples were made at P/SL values varying between 0 and 80. For each P/SL, a blank containing buffer and SL-HE but no peptide was obtained and subtracted from the peptide signal to correct for the background signal. Peptide α-helicity was calculated using the ellipticity at 222 nm and assuming an ellipticity of −32 000 deg·cm^2/dmol for a perfect α-helix.[85,86] The molar ellipticity obtained at 222 nm was used to plot binding isotherms, which were then fit in Excel to obtain the binding dissociation constant, K_d. A two-state model (bound or unbound state of P1/3) was assumed.[78]

Preparation of Samples for Solution NMR

The buffer for solution NMR analysis containing 10 mM phosphate and 25 mM NaCl was prepared in deionized water, lyophilized, resuspended in 99.98% D$_2$O (Cambridge Isotope, Tewksbury, MA), and adjusted to pH 7.4 with 1 M HCl. SL-HE solutions were prepared immediately prior to NMR analysis at concentrations of 280, 700, 1400, and 2800 μM by dissolving powdered SL-HE in NMR buffer. NMR samples containing the P3 peptide were prepared by aliquoting a peptide stock solution in H$_2$O to provide a final concentration of 35 μM peptide (the stock concentration was determined by amino acid analysis). Five samples with peptides were prepared where the P3 peptide stock was diluted in NMR buffer and added to the SL-HE solutions at 280, 700, 1400, and 2800 μM to yield mixtures where the P/SL values were 1:8, 1:20, 1:40, and 1:80. Samples were prepared such that 10% of each sample contained D$_2$O. Samples were kept in warm water to increase their stability prior to NMR analysis.

Solution NMR Experiments

NMR studies were conducted at 310 K using a 600 MHz Bruker AVII system equipped with a 5 mm cryogenically cooled inverse-detection probe with z-axis gradients. Diffusion-ordered spectroscopy (DOSY) measurements were acquired using the pseudo 2D stimulated echo sequence stebpgp1s19 from the Bruker pulse sequence library employing 3−9−19 water suppression, a diffusion period of 300 ms (capital delta), and a 2.2 ms Sine shaped gradient encoding pulse (lowercase delta). The 90° pulse width was 9 ± 0.5 μs, depending on the sample. Sixty four subspectra were acquired with the gradient encoding pulse varying linearly from approximately 4 to 49 G/cm. Data were processed and diffusion coefficients fitted using the Topspin 3.5 software package.

Preparation of Oriented Samples for Solid-State NMR

Oriented samples were prepared to compare the structural and orientational features of P1 and P3 in the absence and presence of SL-HE. Aligned lipid bilayer preparations were made following a protocol that we previously described.[45,71,77] Briefly, the samples were made using 3:1 POPC/POPG. The lipids were mixed in chloroform prior to evaporation of the solvent using nitrogen gas and lyophilization overnight. This lipid film was hydrated with 10 mL of phosphate buffer (3 mM, pH 7.4) containing either P1 or P3 and SL-HE at P/SL = 1:8 based on the CD-monitored titration and SPR results showing strong interactions under these conditions. About 2 mg of each peptide was used per peptide-containing sample, corresponding to about 20 mg of phospholipids and L/P = 20:1. The mixture was swirled to fully suspend the lipids and incubated overnight at 40 °C to allow the peptide, phospholipids, and SL-HE to reach equilibrium. After overnight binding, the samples were centrifuged at 23 700 rpm (Beckman centrifuge with SW40Ti rotor), and the pellet was spread on thin glass slides (dimensions of 5.7 × 12 × 0.03 mm^3 from Matsunami Trading Co., Japan). Each sample was composed of 30−35 slides. Next, the samples were placed in a humidity chamber (>90% using a saturated potassium sulfate solution) until equilibrium was reached. The slides were then rehydrated at a ratio of 1 μL of buffer for every mg of peptide/phospholipid mixture. After stacking, the glass slides were inserted in a glass cell (New Era, Vineland, NJ), sealed with a glass slide and Hampton Research beeswax (Fisher Scientific, Hampton, NH), and incubated at 40 °C until homogeneous hydration was achieved. Control samples included (1) pure POPC/POPG bilayers; (2) POPC/POPG bilayers exposed to SL-HE only in the hydration step; (3) POPC/

POPG bilayers with P1 or P3 but not SL-HE added in the hydration step.

^{31}P Solid-State NMR Experiments

1D ^{31}P spectra were collected on a 600 MHz Bruker Avance 1 spectrometer at the National High Magnetic Field Laboratory (NHMFL). Parameters included a resonance frequency of 242.9 MHz and a 3 μs 90° pulse on ^{31}P and ^{1}H decoupling. The sample temperature was maintained at 32 °C, and 64 scans were averaged with a delay of 3 s between scans. The data were processed with 50 Hz of linebroadening and referenced to phosphoric acid (85% solution).

^{15}N Solid-State NMR Experiments

2D heteronuclear correlation (HETCOR) spectra were recorded on a 750 MHz wide bore Bruker instrument with Avance 1 console at William & Mary. The data were collected using parameters previously used on piscidin samples.[87] For each spectrum, a recycle delay of 5 s and 32−48 t_1 increments with 896 transients each were used. During data acquisition, the temperature settings were 32 ± 0.1 °C. A ^{1}H radiofrequency amplitude of 83.0 kHz was applied during the MSHOT ^{1}H homonuclear decoupling[88] in the t_1 (^{1}H) dimension and during SPINAL decoupling in the t_2 (^{15}N) dimension. A dwell time of 42.6 μs in the indirect dimension was implemented by setting the delay τ_d to 6.3 μs. To observe the ^{15}N/^{1}H dipolar interaction in the indirect dimension, we did not apply ^{15}N RF pulses during the proton evolution in the t_1 dimension. To enhance the detection of this dipolar coupling, the ^{1}H carrier frequency was centered on the amide proton region of piscidin in oriented samples (i.e., ~15 ppm). To transfer the magnetization from the amide proton to its closest ^{15}N spin, a WIM-12 (windowless isotropic mixing) sequence was used with a ^{1}H and ^{15}N radiofrequency amplitude of 55 kHz and a short mixing time (~100 μs). Data were processed with 50 Hz linebroadening in the ^{15}N dimension.

X-ray Diffraction

The samples prepared for the EIS-MS described above were also analyzed by X-ray diffraction (XRD). At the time of analysis, 200 μL of the samples solubilized in 1:1 water:methanol were spread on thin glass coverslips. The bulk water slowly evaporated when the samples sat overnight at room temperature. Before performing the diffraction experiments, the samples were allowed to anneal at 98% relative humidity and room temperature for at least 12 h. X-ray diffraction measurements were carried out on a 3KW Rigaku Smartlab diffractometer (Wilmington, MA) at the Institute for Bioscience and Biotechnology Research (IBBR), Rockville, MD. Phases of the structure factors were characterized using the swelling method.[89] Structure factors were calculated from the integrated Bragg intensities after removing the background and applying Lorentz, polarization, beam footprint, and absorption corrections. Electron density profiles were displayed on an arbitrary scale, using direct Fourier reconstruction.[90]

■ RESULTS

Synergistic Antimicrobial Effect between SL-HE Mixed with Either P1 or P3

To investigate the possible synergy between the antimicrobial effects of HDPs and sophorolipids, we measured the antimicrobial activities of P1/3 and SL-esters (SL-BE and SL-HE) independently and in combination. Minimum inhibitory concentrations (MICs) were measured on Gram-positive *Bacillus cereus* (*B. cereus*) and summarized in Table 1. The MIC values obtained here for P1, P3, SL-BE, and SL-HE are 2, 4, 12, and >200 μM, respectively, and in agreement with previous reports.[43−45,47,64]

Next, we employed the checkerboard experiment to obtain fractional inhibitory concentrations (FICs) and determine whether the peptides and glycolipids act synergistically. By definition, P1 and P3 are 100% inhibitory above their MICs, and thus, the checkboards show complete inhibition for all rows

Table 1. Minimum Inhibitory Concentration of P1, P3, and SL-HE against Mid-Log Phase Pathogens

MIC (μM)	piscidin 1	piscidin 3	SL-HE
B. cereus	2	4	>200[a]
S. aureus	2	2	>200
E. coli	4	>6	>200

[a]Ref 64.

where the peptides are plated at or above their MICs (Figure 2). As indicated by the abrupt change in color from dark to light, the MIC is highly sensitive to the peptide concentration, displaying the ability of these peptides to act cooperatively to perform their function.[91,92] When P1 is 0.5 μM, an increase in the SL-HE concentration from 4 to 8 μM abruptly changes the inhibitory effect from 0 to 100%, resulting in a 4-fold decrease in the MIC value. In the next row where P1 = 1 μM, a similar abrupt transition and shift to a lower MIC value relative to peptide alone are observed when the SL-HE concentration reaches 2 μM. In the case of P3, peptide concentrations as low as 0.5 and 1 μM become inhibitory in the presence of SL-HE at 8 μM, demonstrating an 8-fold and 4-fold decrease, respectively, in effective MIC value relative to P3 peptide alone. When [P3] = 2 μM, a more gradual increase in the inhibitory effect is detected when the SL concentration reaches 1 μM, with full inhibition at 4 μM.

Based on our experimental approach, obtaining an FIC index ≤0.50 is interpreted as evidence for synergy between the two compounds.[93] Thus, the results summarized in Figure 2 indicate that synergy exists between P1/3 and SL-HE. The best FIC value for P1 is 0.25 obtained when P1/SL-HE = 0.5 μM/8 μM = 1:16 and 0.5 μM/16 μM= 1:32. For P3, it is 0.12 obtained when P3/SL-HE = 0.5 μM/8 μM = 16 and 0.5 μM/16 μM = 32. Synergy extends to an FIC value of 0.50 for P1 (e.g., P1/SL-HE = 1 μM/2 μM = 1:2 and 1 μM/4 μM = 1:4). For P3, FIC values of 0.25 (e.g., P3/SL-HE = 1 μM/8 μM = 1:8) and 0.50 (e.g., P1/SL-HE = 2 μM/4 μM = 1:2) are also observed. Results for piscidin with the SL butyl ester also show shifts to a lower effective MIC value relative to peptide alone (data not shown). However, higher FIC values were obtained likely due to SL-BE alone having a lower MIC (12 μM) on *B. cereus* relative to SL-HE,[64] and thus, the overall synergistic effects are more striking with SL-HE. Overall, these assays indicate that strong synergistic antimicrobial effects exist between SL-HE combined with either P1 or P3.

Permeabilization Assays on Bacterial Cells Exposed to SL-HE Mixed with Either P1 or P3

Given previous studies of P1 and P3 demonstrating their ability to permeabilize bacterial and model membranes,[47] we investigated whether SL-HE could also damage the plasma membranes of bacteria. A dye leakage assay was performed on *B. cereus* in the presence of SL-HE and P1 and P3. As shown in Figure 3, the leakage data obtained with the diS-C3 dye occur in a dose-dependent fashion. Overall, P1 shows a higher ability than P3 to permeate bacterial membranes at a given peptide concentration, which is consistent with previous work.[47] Interestingly, combinations of P1-SL-HE and P3-SL-HE induce higher permeability than P1 and P3, respectively, suggesting that the enhanced antimicrobial effects of piscidin in the presence of SL-HE may be due to an increase in the permeabilization capability.
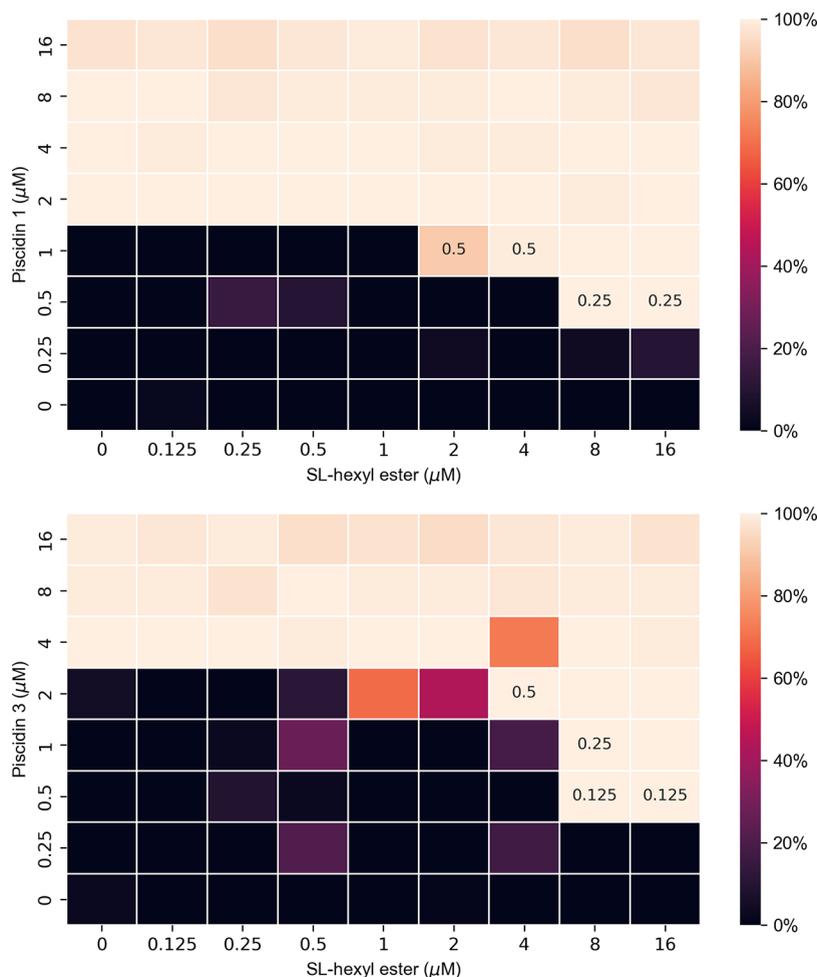
Figure 2. Synergy antimicrobial testing of SL-HE with either P1 or P3 on *B. cereus*. A schematic representation is displayed for the checkerboard results obtained when *Bacillus cereus* (ATCC 4342) was incubated for 16 h in the presence of piscidin 1 (P1), piscidin 3 (P3), and/or sophorolipid hexyl ester (SL-HE). Either P1 (top) or P3 (bottom) was mixed with the SL-HE at the indicated concentration. The color scheme indicated on the right-hand side is used to represent the inhibition rate in each well. The percentages are based on OD measurements that are normalized with respect to the controls to span the 0–100% range.
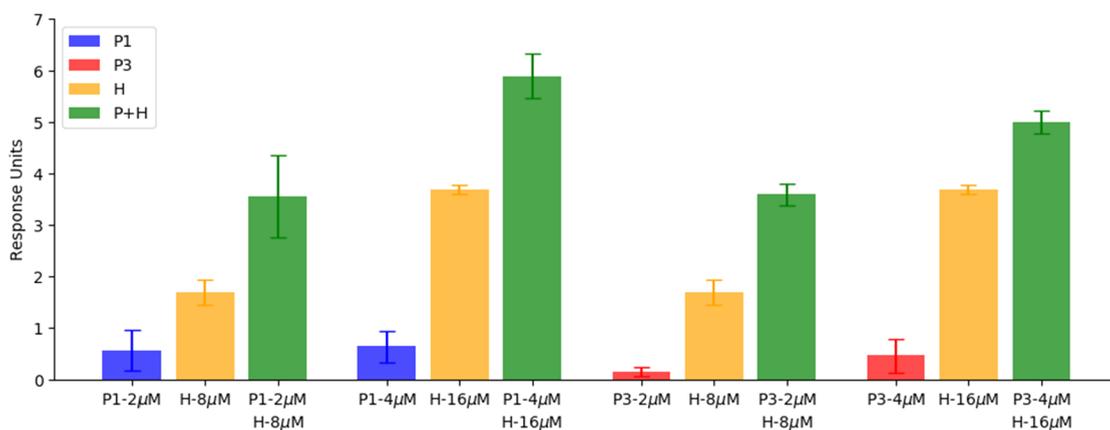
Figure 3. Permeabilization effects of P1, P3, SL-HE, and SH-HE with either P1 or P3 on *B. cereus*. The data were collected on *B. cereus* grown to mid-log phase at the indicated concentration of piscidin 1 (P1), piscidin 3 (P3), and SL-HE (H). The diS-C3 fluorescence probe was used to monitor leakage. The response units on the vertical axis correspond to the fluorescence of the samples normalized against that obtained with the PBS negative control.

Permeabilization Assays on Synthetic Phospholipid Vesicles Exposed to SL-HE Mixed with Either P1 or P3

The release of calcein from synthetic liposomes is a well-established method to characterize membrane permeabilization effects of membrane-active peptides.[94−96] The peptides trigger permeabilization once they reach a certain threshold concentration, which depends on the peptide sequence, membrane composition, and experimental conditions (e.g., pH). On a

mechanistic level, the threshold for activity, typically measured as a lipid-to-peptide molar ratio (L/P), correlates with the conditions that lead a given peptide to reorient and insert more deeply in membranes. The sigmoidal shape of the dose-dependent curves is indicative of a cooperative effect between peptide molecules when the threshold concentration is reached. In this study, we used 3:1 (mol/mol) 1-palmitoyl-2-oleoyl-*sn*-glycero-3-phosphocholine (POPC)/1-palmitoyl-2-oleoyl-*sn*-glycero-3-phosphoglycerol (POPG) to mimic the membrane charge content of bacteria, such as the *B. cereus* used in the MIC assays.[75] Large unilamellar vesicles (LUVs) were made with this lipid composition with calcein trapped inside. For P1 and P3 either alone or in combination with SL-HE, dose-dependent curves were constructed by quantifying the amount of calcein release as a function of L/P. For the assays where piscidin was combined with SL-HE, the peptide-to-SL-HE molar ratio (P/SL) was fixed at 1:8, which is in the middle of the range where synergy is observed in the MIC assays (Figure 2). As demonstrated in Figure 4, not only P1 and P3 but also SL-HE permeabilize the LUVs used for this assay.
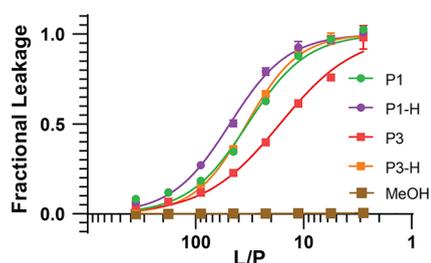
Figure 4. Permeabilization effects of P1, P3, SL-HE, and SL-HE with either P1 or P3 on 3:1 POPC/POPG vesicles. Vesicles at a fixed concentration of 42 μM lipid were exposed to increasing amounts of P1 and P3 in the absence and presence of SL-HE (H). The fractional leakage of calcein from POPC/POPG liposomes is plotted as a function of the lipid-to-peptide ratio (L/P). The EC$_{50}$ values as L/P values are as follows: 32 for P1; 48 for P1 + SL; 17 for P3; 35 for P3 + SL. When the POPC/POPG vesicles were treated with only SL-HE, the EC$_{50}$ = 2 as a lipid-to-SL-HE ratio (L/SL) (Figure S1). The SL was dissolved in methanol before being added to the wells; therefore, a negative control was run with an equivalent amount of methanol. The assays were repeated three times in triplicate, with the data shown corresponding to the mean ± SD for a representative data set. The error bar in some cases is smaller than the symbols used to represent the data points.

The L/P values that result in 50% leakage (EC$_{50}$) provide a useful way to quantify the activities of the peptides. The EC$_{50}$ values (L/P1 = 42 μM/1.3 μM = 32 and L/P3 = 42 μM/2.5 μM = 17), obtained in the absence of SL, agree well with those previously determined using 3:1 POPC/POPG, with P1 being more active than P3.[50] Alone, SL-HE is also slightly membrane active, with EC$_{50}$ occurring at a lipid-to-sophorolipid ratio (L/SL) equal to 42 μM/21 μM = 2 (Figure S1). In combination with SL-HE at the molar ratio of 1:8, P1 and P3 exhibit enhanced membrane permeabilization ability (L/P1 = 42 μM/0.88 μM = 48; P3/L = 42 μM/1.2 μM = 35). Overall, the model membrane system captures well the permeabilization trends seen in the antimicrobial assays: P1 is more membrane active than P3, and SL-HE is only weakly membrane active on its own. Importantly, combining SL-HE with either P1 or P3 increases the ability of the peptides to permeabilize model membranes. In the context of bacterial cell membranes, the peptides could act by not only disrupting the membranes but also accessing intracellular

targets.[46,47] Next, additional biophysical studies were performed to gain deeper insight into the mechanism underlying the synergy between each piscidin and SL-HE.

Mass Spectrometry of Phospholipid Bilayers Exposed to SL-HE and Piscidin

The dye leakage assays on live cells and model membranes indicate that not only P1/3 but also SL-HE disrupt membranes. It is well-known that HDPs have strong affinity for lipid bilayers. However, less is known about SL-ester/phospholipid interactions. Mass spectrometry (MS) was used qualitatively to determine whether SL-HE can associate with phospholipid bilayers. Quantitative measurements of lipid concentrations to determine partitioning coefficients would require isotopically labeled internal lipid standards and a triple quadrupole mass spectrometer to perform a liquid chromatography (LC)-MS/MS multiple-reaction monitoring assay, an approach that can provide coefficients of variance <5%.[97,98] After mixing the phospholipids with SL-HE in the presence and absence of peptide at L/P = 20:1 and P/SL = 1:8, the samples were centrifuged, so that the pelleted phospholipid portion and supernatant could be separately probed by MS. As shown in Figures 5 and S2, SL-HE binds to phospholipid membranes
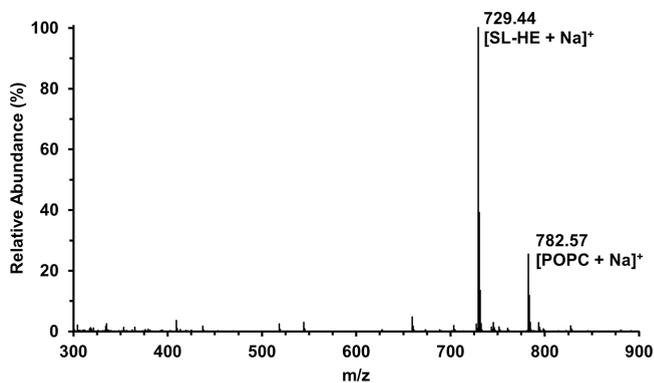
Figure 5. Mass spectrometry data collected on phospholipid bilayers exposed to SL-HE. To investigate the ability of SL-HE to interact with phospholipid bilayers, three samples were made, including a 3:1 POPC/POPG sample with P1 and SL-HE at L/P = 20:1 and P/SL = 1:8 and its control counterparts: a 3:1 POPC/POPG blank; a 3:1 POPC/POPG sample with SL-HE but no P1. Suspensions of 3:1 POPC/POPG were prepared in a phosphate buffer. After overnight incubation in buffer in the absence or presence of SL-HE or SL-HE/P1, the samples were centrifuged, and the pellets as well as supernatant were analyzed by electrospray ionization mass spectrometry (ESI-MS). The spectrum shown above is for the pellet from the 3:1 POPC/POPG sample with SL-HE, as observed in the positive ion mode. The main peak at m/z = 729.44 corresponds to [SL-HE + Na]$^+$ while the other major peak at m/z = 782.6 indicates [POPC + Na]$^+$. Figure S2 displays additional data collected in the positive and negative modes on other samples, including the 3:1 POPC/POPG blank and the 3:1 POPC/POPG sample with P1 and SL-HE.

(pelleted part of the sample) whether it is used alone or in combination with P1/3. This reveals the ability of this glycolipid to establish interactions with essential constituents of cell membranes rather than to stay in solution.

Interactions of Phospholipid Bilayers Exposed to SL-HE Mixed with Either P1 or P3 as Determined by Surface Plasmon Resonance

As shown by the MS data and permeabilization assays with live cells and model membranes, not only P1/P3 but also SL-HE
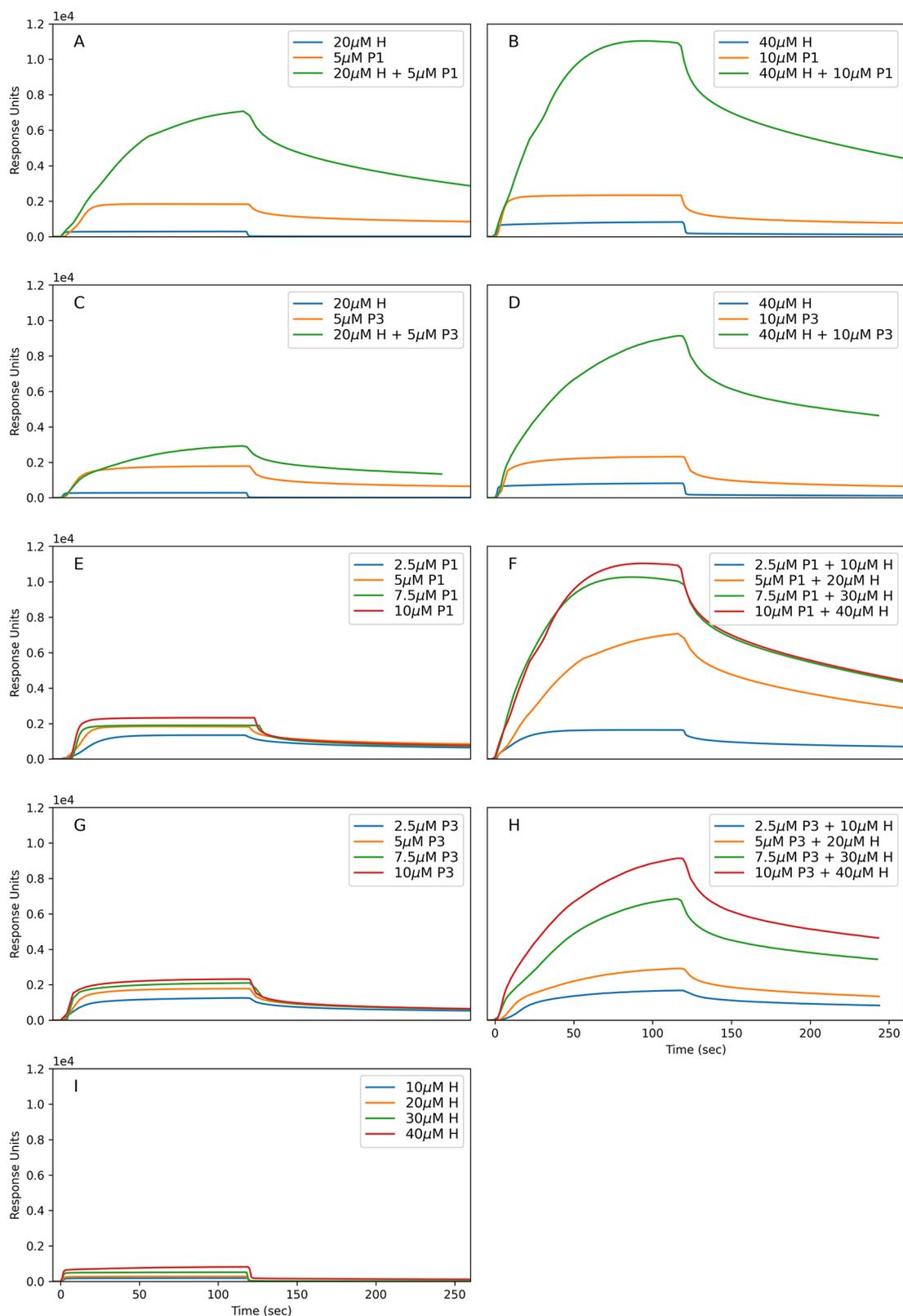
Figure 6. Sensorgrams for 3:1 POPC/POPG bilayers exposed to P1, P3, SL-HE, and SL-HE with either P1 or P3. Small unilamellar vesicles were deposited on the L1 sensor and allowed to form supported lipid bilayers (SLBs). After the SLB was washed, the peptide solution was flown onto the bilayer. The graphs show the data collected upon addition of P1, P3, and/or SL-HE (H) at different concentrations: (A) 5 μM P1 and 20 μM SL-HE mixture; (B) 10 μM P1 and 40 μM SL-HE mixture; (C) 5 μM P3 and 20 μM SL-HE mixture; (D) 10 μM P3 and 40 μM SL-HE mixture; (E) P1 at 4 concentrations; (F) P1 and SL-HE mixture at 4 concentrations; (G) P3 at four concentrations; (H) P3 and SL-HE mixture at four concentrations; (I) SL-HE at four concentrations.
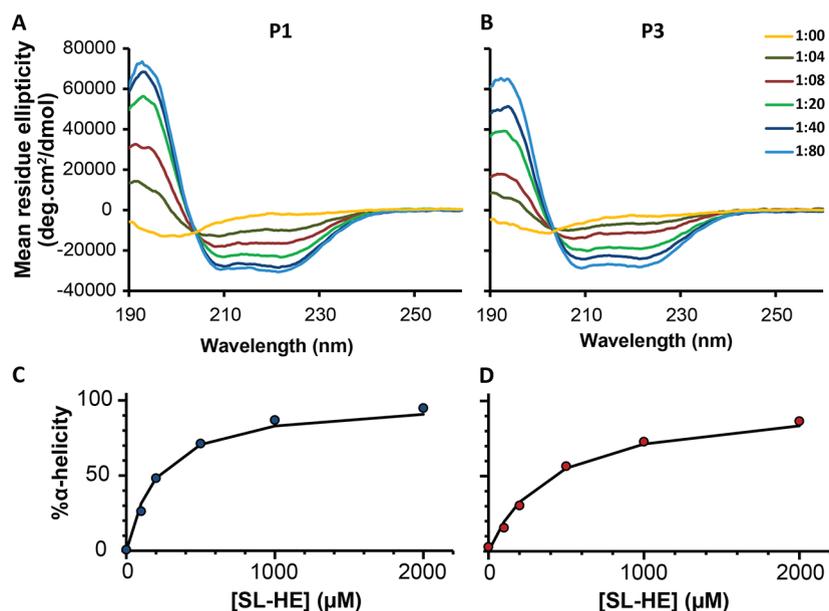
Figure 7. Secondary structure monitoring of P1 and P3 as a function of the SL-HE concentration. CD data for P1 (A) and P3 (B) are plotted as a function of the indicated P/SL values. The α-helical content deduced from the CD data is plotted as a function of [SL-HE] and fitted to obtain the dissociation constant (K_d) for the complex between SL-HE and either P1 (C) or P3 (D). The peptide concentration was fixed at 25 μM, with the SL-HE concentration varied from 0 to 2 mM. The experimental data points are in dark blue for P1 and red for P3. The fits calculated based on a simple two-state equilibrium between each peptide and SL-HE are represented by the solid lines. Based on duplicates, the K_d values and standard errors obtained for P1 and P3 are 206 $\pm$ 5 and 392 $\pm$ 2 μM, respectively.

interact with membranes. Since we cannot deduce from the MS data the extent to which the peptide and SL-HE bind to phospholipids, we used surface plasmon resonance (SPR) to monitor the accumulation of the peptides within 3:1 POPC/POPG membranes, with and without preincubation with SL-HE.

Figure 6 displays the sensorgrams obtained for P1, P3, and SL-HE interacting with a supported lipid bilayer (SLB) made of 3:1 POPC/POPG, the same model membranes used in the dye leakage assays. First, analyte solutions containing P1, P3, SL-HE, or combinations thereof were flowed onto the SLB. Subsequently, the analyte free buffer solution was used during the washing step to dissociate loosely bound analytes from the SLB. While the SLB interacts strongly with P1 and P3 in agreement with previous studies,[50,53] the interactions with SL-HE are weak. P1 and P3 give rise to distinct association (increase in the RU value) and dissociation (decrease in the RU value) phases. Next, P1/3 was preincubated with SL-HE at P/SL = 1:4 before adding the complex to the SLB. As shown in Figure 6, a massive accumulation of material is observed on the sensor when the P1/SL-HE and P3/SL-HE complexes were flowed onto the SLB. The RU signal at the end of the washing step remains very high, indicating a very slow dissociation from the SLB and, thus, a strong interaction. Across all tested concentrations leading to the P/SL value of 1:4 piscidin and SL-HE, bilayer accumulation is stronger by a factor of at least 5-fold compared to when only P1 or P3 is loaded onto the SLB. Since SL-HE alone accumulates only slightly on the SLB, this highlights the synergistic accumulation when P1/3 and SL-HE are both present.

How the presence of SL-HE impacts the kinetics of association and dissociation of piscidin with membranes was investigated as previously performed for P1/3 alone binding to the SLB.[50] In that previous work, membrane association was found to follow pseudo-first-order kinetics based on the apparent rate constant k_{obs}^{on} increasing with a linear dependence

in peptide concentration. Here, apparent rate constants for dissociation also increased with increasing peptide concentration, suggesting that, as the membranes become saturated with peptide, electrostatic repulsion between peptide molecules increases and drives dissociation. However, binding data with P1/SL-HE and P3/SL-HE combinations show these rate constants slightly decrease rather than increase as a function of peptide concentration (Figure S3). When SL-HE was used alone, no significant interaction was measured with the SLB. Taken together with the observation that the maximum RU signal observed for P1/3 was generally 5-fold higher in the presence of SL-HE, this may indicate that SL-HE introduces new membrane binding modes for P1 and P3 that have slower on and off rates.

Overall, the SPR data are insightful in several ways. First, they reveal that, when P1 and P3 are preincubated with SL-HE, they synergistically accumulate onto bilayers. P1 accumulates more strongly than P3, in accordance with its stronger antimicrobial and permeabilization effects. Furthermore, the enhanced membrane accumulation achieved when piscidin and SL-HE are coadded correlates with the boosted antimicrobial and permeabilization effects observed for their combinations (Figures 3–5). Second, the SPR data suggest that a new mode of peptide−bilayer interaction applies when SL-HE is present. Mechanistically, this could mean that the molecular structure of the peptide−lipid assemblies could be different when SL-HE is present. To explain the different modes of peptide−membrane interactions when SL-HE is present and the synergistic membrane accumulation of piscidin and SL-HE, we postulated that (i) piscidin binds to the micelles formed by SL-HE, prefolding the peptide into its active state before it reaches the membrane and concentrating it for enhanced membrane delivery; (ii) once SL-HE is incorporated into the phospholipid bilayer, it recruits the peptide to the membrane by using its sugar moiety or forming defects that alter the membrane order or
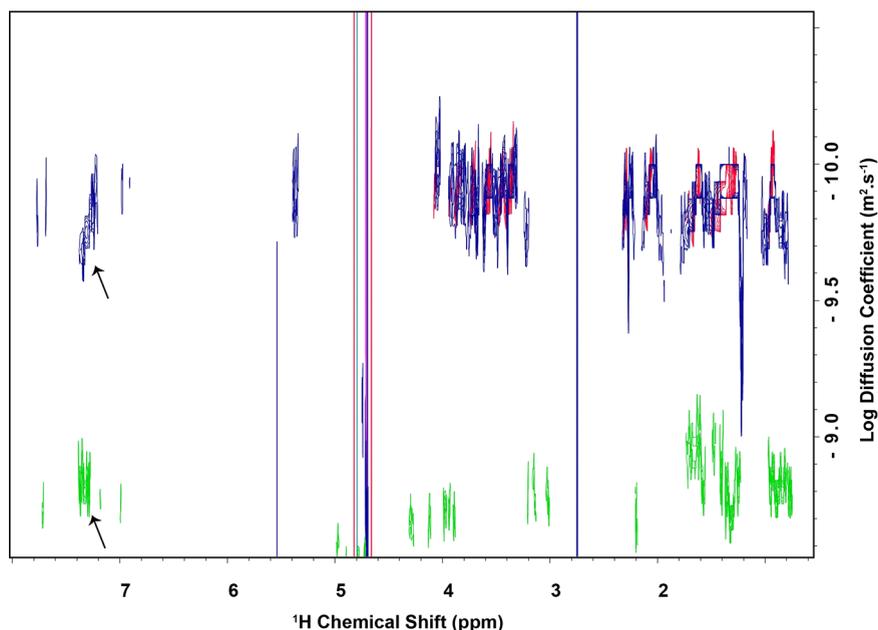
Figure 8. DOSY data were collected to characterize SL-HE micelles in the absence and presence of piscidin 3. Diffusion-ordered spectroscopy (DOSY) spectra were collected at 37 °C to investigate SL-HE and P3 association. An overlay of DOSY spectra is shown for P3 alone (green), 280 μM SL-HE alone (red), and a mixture of P3/SL-HE at P/SL = 1:8 (blue). Black arrows indicate resolved P3 signals detected in spectra of the P3 alone and the P3/SL-HE samples that are absent in spectra of the SL-HE alone sample. The diffusion coefficient for the peptide alone is detected to be an order of magnitude greater than that of SL-HE micelle and becomes equivalent to that of the micelle when P3 and SL-HE are combined, indicating that the peptide directly interacts and diffuses along with the micelles with minimal perturbation to the diffusion properties of the micelle.

curvature. To interrogate this hypothesis, the following section describes studies that were done by circular dichroism (CD), NMR, and X-ray diffraction to gain further insights into structures formed as a result of the interactions between P1/3-SL-HE.

Formation of P1/SL-HE and P3/SL-HE Complexes as Monitored by Circular Dichroism

CD was used to probe whether binding of SL-HE to P1/P3 results in significant peptide conformational changes. Indeed, HDPs such as piscidin, which are unstructured in solution, typically fold into amphipathic structures in the presence of an amphipathic surface. Given these tendencies, we used CD to measure the α-helical content of the peptides as a function of the SL-HE concentration. The ellipticity at 222 nm was used to calculate α-helicity assuming that the ellipticity for a perfect α-helix is $-32\,000$ deg·cm^2/dmol.[85,99] Figure 7A,B shows the mean residue ellipticity of P1 and P3 when the peptides are titrated with SL-HE from P/SL = 1:0 to 1:80. Since the peptides were used at a fixed concentration of 25 μM, this corresponds to a concentration of SL-HE that varies from 0 to 2 mM. With increasing levels of SL-HE, the positive band at 196 nm increases, while the negative band at 222 nm becomes increasingly negative, indicating an increase in α-helical content. Peptide α-helicity is plotted in Figure 7C,D as a function of the SL-HE concentration.

Based on the FIC data reported above (Figure 2), synergy is achieved when the piscidin/SL-HE molar ratio ranges from 1:2 to 1:32. When P1/SL-HE = 1:8 (middle of the range for the synergy), the α-helical content of the P1 sample is about ∼50%, while at P1/SL-HE = 1:80, it is close to 100%. In contrast, increasing the P3/SL-HE ratio from 1:8 to 1:80 results in α-helical contents of about 30% and 80%, respectively. Thus, antimicrobial synergy occurs in the range where SL-HE can shift the conformation of the peptides. The titration data shown in

Figure 7 feature a distinct isosbestic point, pointing at the presence of two states, one that is unstructured and another one that has α-helical character. Previous structural studies by solid-state and solution NMR have showed that the conformation adopted by piscidin in the presence of lipid bilayers and lipid mimetics is fully α-helical.[49,77,86] Assuming that piscidin also becomes fully α-helical when it binds to SL-HE micelles, the α-helical content plotted in Figure 7 reflects the amount of peptide bound to the sophorolipid. To compare more quantitatively the behaviors of P1 and P3 as they bind to SL-HE micelles, these CD data were fitted to the bimolecular binding equation, which assumes a one binding site model. This yielded dissociation constants K_d of 206 ± 5 μM for P1 (Figure 7C) and 391.5 ± 1.5 μM for P3 (Figure 7D). These results reveal that both P1 and P3 noncovalently interact or associate with SL-HE, with P1 featuring a stronger affinity. Importantly, these experiments provide evidence that SL-HE directly interacts with P1/3. This interaction promotes a change in peptide conformation in the range of P/SL ratios that are relevant to the antimicrobial synergy observed in Figure 2.

Solution NMR on SL-HE Aggregates Exposed to Piscidin

Having demonstrated that piscidin binds to SL-HE, we conducted a study to determine whether the properties of SL-HE micelles are influenced significantly by the peptides. For this purpose, we used diffusion-ordered spectroscopy (DOSY), a form of solution NMR that relies on gradients to measure the translational diffusion coefficients of molecules in solution.[100] SL-HE is expected to form micelles above 2.84 μM at 36 °C, based on a previous determination of the CMC in water.[67] DOSY measurements were performed here with P3 only since P1 and P3 behaved similarly in the biological assays and CD binding experiments, and thus, their modes of interactions with the SL micelles could be assumed to be similar. Figure 8 shows examples of 2D DOSY spectra acquired at 37 °C for P3

interacting with SL-HE at a P/SL = 1:8. These 2D DOSY spectra are generated as series of 1D ^{1}H diffusion weighted subspectra with the signal appearing in each according to its fitted diffusion coefficient. Based on the DOSY results, the diffusion coefficient of SL-HE at 280, 1400, and 2800 μM were estimated to be -9.9, -9.9, and $-10 \log(\text{m}^2 \cdot \text{s}^{-1})$, respectively (Table 2). Since micelle

Table 2. Diffusion Coefficients for P3 and SL-HE

P3 concentration (μM)	SL-HE concentration (μM)	diffusion coefficient [$\log(\text{m}^2/\text{s})$]
35	**0**	**−8.8**
0	2800	−10
35	**2800**	**−10**
0	1400	−9.9
35	**1400**	**−9.8**
0	700	N/A
35	**700**	**−10**
0	280	−9.9
35	**280**	**−9.9**

size and therefore diffusion coefficients are expected to be largely independent of SL-HE at concentrations substantially above the CMC, the small apparent changes in the coefficient value when the SL concentration is increased are very likely the result of reduced diffusion due to transient aggregation and/or molecular crowding at higher micelle concentrations. The diffusion coefficient for P3 at 35 μM was calculated to be approximately $-8.8 \log(\text{m}^2 \cdot \text{s}^{-1})$, greater than an order of magnitude faster compared to the range of values found for the SL-HE micelles. Analysis of diffusion coefficients for solutions of 35 μM P3 with 280, 700, 1400, and 2800 μM SL-HE (corresponding to P3/SL-HE = 1:8, 1:20, 1:40, and 1:80, respectively) gave values of -9.9, -10, -9.8, and $-10 \log(\text{m}^2 \cdot \text{s}^{-1})$. Importantly, the ^{1}H resonances of both the P3 peptide and SL-HE are detected within the same subspectra of the 2D DOSY data sets, and therefore are determined to have equivalent diffusion coefficients when they are exposed to each other. Overall, the change in diffusion behavior that occurs for P3 in the presence of SL-HE micelles corroborates the CD studies by showing that piscidin interacts with the SL-HE micelles.

^{31}P Oriented Sample Solid-State NMR on Phospholipid Bilayers Exposed to SL-HE Mixed with Either P1 or P3

Oriented sample solid-state NMR (OS SS-NMR) was then used to investigate how the presence of SL-HE influences the bilayer organization and the structural features of the peptides. ^{31}P is present at high natural abundance in the phospholipids; thus, no isotopic enrichment is needed. For the peptides, ^{15}N was incorporated into the amide bond at position 13. Using ^{31}P and ^{15}N detection, the phospholipids and peptide were followed, respectively. First, the results from the ^{31}P experiments are discussed.

^{31}P OS SS-NMR is a powerful method to investigate the mechanisms of action of membrane-active peptides on a molecular level.[101−107] Aligned bilayers are prepared in the absence and presence of peptide, and the oriented ^{31}P chemical shift signals are interpreted in terms of their position and line width. This method was used here to reveal if the association of P1/3 with SL-HE prior to exposing the peptide to the phospholipids could result in stronger membrane disruption. For this purpose, samples were prepared where the peptide and SL-HE were allowed to associate with each other before being exposed to 3:1 POPC/POPG bilayers. We used P/SL = 1:8 and

L/P = 20:1 based on the CD-monitored titration and SPR results showing strong interactions under these conditions.

Figure 9 shows the ^{31}P spectra obtained for hydrated 3:1 POPC/POPG bilayers exposed to ^{15}N[G$_{13}$]-P1 and ^{15}N[G$_{13}$]-
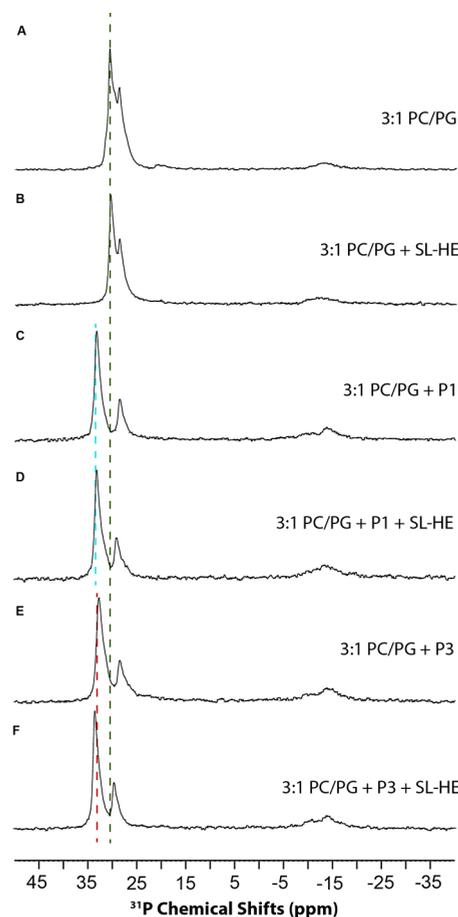
Figure 9. ^{31}P solid-state NMR spectrum of hydrated oriented 3:1 POPC/POPG lipid bilayers in the presence and absence of P1, P3, and SL-HE. The following conditions were tested: (A) pure 3:1 POPC/POPG; (B) 3:1 POPC/POPG exposed to SL-HE; (C) 3:1 POPC/POPG exposed to P1; (D) 3:1 POPC/POPG exposed to P1 preincubated with SL-HE; (E) 3:1 POPC/POPG exposed to P3; (F) 3:1 POPC/POPG exposed to P3 preincubated with SL-HE. The vertical lines are used to facilitate the comparison of the spectra: the green line is placed on the tallest peak in the 3:1 POPC/POPG sample; the blue (red) line is used to compare P1 (P3) spectra with and without preincubation with SL-HE. The peptide-containing samples were made using ∼2 mg of either P1 or P3. The samples containing piscidin and SL-HE were made at L/P = 20:1 and P/SL-HE = 1:8. The other samples were made as direct counterparts lacking the SL-HE and/or peptide. The samples were placed in the NMR coil with the bilayer normal parallel to B$_0$. The spectra were recorded at a frequency of 242.9 MHz at 32 °C, above the lipid phase transition temperature.

P3 preincubated or not with SL-HE. We had previously used 3:1 1,2-dimyristoyl-*sn*-glycero-3-phosphocholine (DMPC)/1,2-di-myristoyl-*sn*-glycero-3-phosphoglycerol (DMPG) as bacterial membranes to obtain the structures and orientations of membrane-bound P1 and P3.[45,71,77] Here, we prepared 3:1 POPC/POPG bilayers and exposed them to SL-HE in the presence or absence of the peptide. In samples of fully hydrated bilayers above their phase transition temperature, the chemical shift anisotropy (CSA) is averaged by motions. In the case of
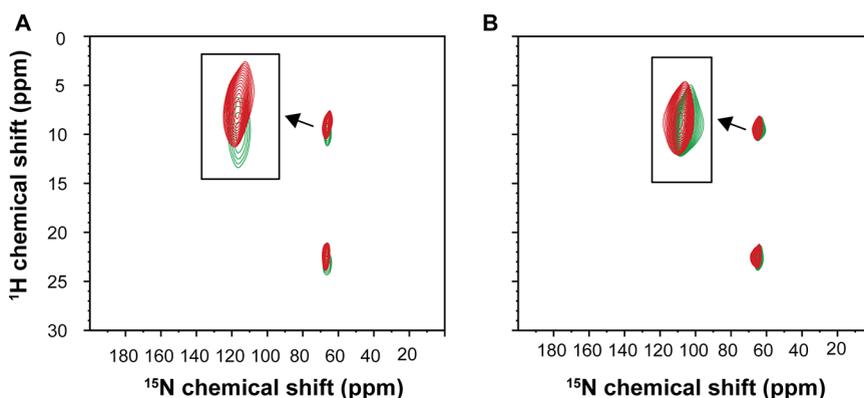
Figure 10. Structural studies of P1 and P3 bound to membranes in the presence and absence of SL-HE. 2-D HETCOR solid-state spectra are shown for ^{15}N-G13-P1 (A) and ^{15}N-G13-P3 (B) preincubated with SL-HE (red) or not (green). A pair of peaks is obtained along the ^{1}H dimension due to the splitting of the ^{1}H amide resonance by the ^{15}N amide nucleus that is coupled through a dipolar interaction (~10 kHz). The inset corresponds to an enlargement of the cross peak next to the arrow, which highlights the small changes in chemical shift that occur when each peptide is preincubated with SL-HE. These peptide-containing samples were made at L/P = 20:1. When present, SL-HE was added at a P/SL = 1:8. The spectra were recorded at 32 °C, above the phase transition temperature of the lipids at ^{1}H and ^{15}N frequencies of 750.3 and 76 MHz, respectively. The samples were placed in the NMR coil with the bilayer normal parallel to B$_0$. The corresponding ^{31}P data from these samples are shown in Figure 9.

phospholipids where lipid molecules experience fast averaging about its long axis, ^{31}P spectra are axially symmetric and characterized by two principal components: $\sigma_{//}$ (~30 ppm) for the molecules oriented with their long axis parallel to B$_0$ and $\sigma_{\perp}$ (~−15 ppm) for the lipids oriented perpendicular to B$_0$. In oriented samples placed with the bilayer normal parallel to B$_0$, as the case in Figure 9, the spectra are dominated by the chemical shift at $\sigma_{//}$ unless bilayer disruption is induced by the constituents.[108−111]

For neat POPC/POPG bilayers, two nonfully resolved resonances in an approximately 3:1 ratio are observed at 31 and 29 ppm, corresponding well to the expected resonances for POPC and POPG, respectively.[78] A weak signal around −15 ppm ($\delta_{\perp}$) is indicative of unoriented bilayers, which arise due to the detection of unaligned lipids on the edges of the glass plates. When P1/P3 is added to the POPC/POPG mixtures at L/P = 20:1, two major changes are observed and interpreted as follows: (1) the dominant signal remains near 28−33 ppm; thus the lipids maintain good alignment; (2) the major peaks move from 31 and 29 ppm to 33 and 28.5 ppm, respectively, and therefore become more resolved. Clearly, the peptide strongly affects the chemical shifts and electronic environment of the lipid headgroups. As described by Seelig, Macdonald, and Scherer through a phenomenon called the "voltmeter effect", when phospholipid headgroups such as PC and PG interact with charged or polar substances, they change their orientation with respect to the bilayer normal, thereby influencing their dipole and the membrane surface charge.[101,112] This voltmeter behavior of phospholipid headgroups in the presence of amphipathic peptides can be detected by ^{2}H and ^{31}P solid-state NMR.[78,101,103,104,112−114] Importantly, Marassi and Macdonald showed using ^{2}H quadrupolar splittings and ^{31}P chemical shifts that the PC headgroup is more sensitive than PG to this membrane surface charge.[115] This is in agreement with the chemical shift changes observed here for POPC and POPG exposed to P1 and P3. Interestingly, we did not notice major changes in ^{31}P chemical shifts when the mixture of phospholipids and peptides at L/P = 20:1 was exposed to SL-HE at P/SL = 1:8. However, minor effects were observed. More specifically, upon addition of SL-HE, the resonance for POPC moves downfield from 28.6 to 29.2 ppm in the POPC/POPG/

P1 sample and from 28.4 to 29.7 ppm in the POPC/POPG/P3 sample. The SL-HE also induces small downfield shifts to POPC in the sample containing P3 since the corresponding resonance moves from 32.7 to 33.6 ppm when the SL-HE lipid is added to the POPC/POPG/P3 sample.

^{15}N Oriented Sample Solid-State NMR of P1 and P3 Bound to Phospholipid Bilayers and Exposed to SL-HE

^{15}N OS SS-NMR was used to investigate peptide structure in the same samples that were used for ^{31}P NMR. To probe not only the chemical shifts but also the ^{15}N−^{1}H dipolar coupling as a sensitive reporter of peptide orientation,[116,117] we collected 2D spectra at L/P = 20:1. As seen in Figure 10, the samples gave rise to excellent signals in both dimensions with the ^{15}N nuclei resonating near 65 ppm. If the peptide was not strongly bound to the bilayers, this solid-state NMR experiment would detect an isotropic ^{15}N signal near 120 ppm.[118] Thus, the peptides are bound to the bilayers present in the sample. The ^{15}N chemical shifts near 65 ppm and ^{15}N−^{1}H dipolar coupling of about 10 kHz are consistent with an α-helical structure laying parallel to the membrane surface, as previously observed in DMPC/DMPG.[45,71,77] This orientation of P1 and P3 is favored given that their amphipathic nature is conducive to partitioning at the water−bilayer interface.[119−121] When SL-HE is present during sample preparation at P/SL = 1:8, small changes in chemical shifts and dipolar couplings are observed, suggesting that the peptide responds to the presence of sophorolipid incorporated into the bilayer due to either direct (e.g., peptide-SL-HE interactions) or indirect effects (e.g., a new conformational arrangement of the peptide produced by SL-HE-induced changes in the bilayer structure). Overall, the CD and NMR data show that P1 and P3 bind to both SL-HE micelles and phospholipid bilayers; however, when they are first bound to SL-HE, they retain their ability to interact with phospholipids without major alteration to their structure and orientation.

X-ray Diffraction of Phospholipid Bilayers Exposed to SL-HE in the Presence of Piscidin

While the MS data (Figure 5) indicate that SL-HE is present in phospholipid bilayers, it does not indicate whether the glycolipid is loosely bound or strongly incorporated inside the bilayer structure. To distinguish between these two cases and

characterize any changes in bilayer organization that could be induced by SL-HE, X-ray diffraction (XRD) was performed. XRD is uniquely suited to characterize the phases of the bilayer and its thickness, both of which could change when a membrane-active substance is present. The XRD data from aligned 3:1 POPC/POPG bilayer stacks (multilayers) shown in Figure 11 display significant changes in both the repeat spacings
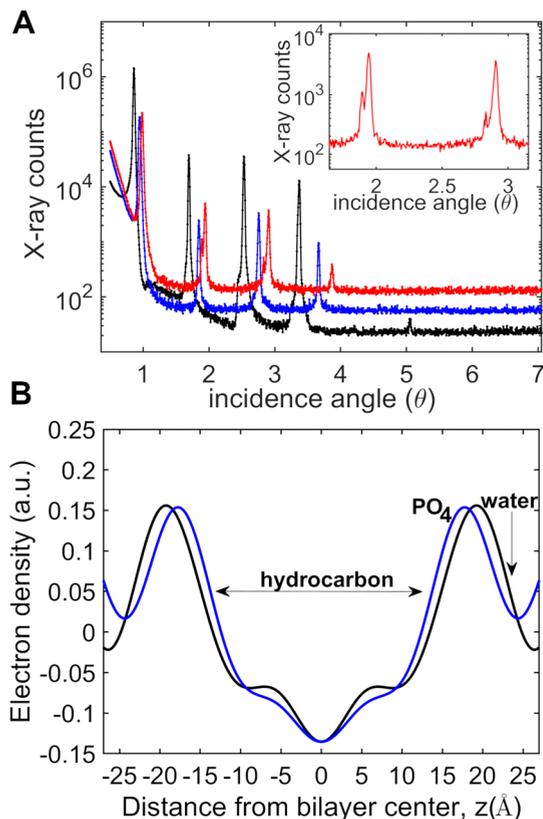
Figure 11. X-ray diffraction data from aligned phospholipid multilayers exposed to SL-HE and P1. (A) One dimensional Bragg diffraction signals probing the direction (z) perpendicular to the bilayer surface. The repeat spacings (d) of the hydrated bilayer stacks are 52.8 ± 0.04 (black, neat 3:1 POPC/POPG); d = 48.8 ± 0.2 (blue, SL-HE + 3:1 POPC/POPG); d = 45.9 ± 0.1 (red, P1 + SL-HE + 3:1 POPC/POPG, major peaks). The inset displays a closeup of diffraction orders 3 and 4 of the red curve, which shows a minor component at a smaller repeat spacing, d = 47.6 ± 0.3 Å. The peptide-containing sample was prepared at L/P = 20:1 and P1/SL-HE = 1:8. The other two samples were prepared as direct counterparts lacking either the SL-HE and peptide or only the peptide. (B) Electron density profile of the bilayer projected on the a-axis for 3:1 POPC/POPG (black) and SL-HE + 3:1 POPC/POPG (blue). The most prominent features are the electron-rich phosphate groups bordering the hydrocarbon region (horizontal arrow). The increase in electron density around the bilayer surfaces for the SL-HE + POPC/POPG sample compared with neat POPC/POPG very likely reflects the presence of the sugar groups on the membrane surface and additional water accumulation (vertical arrow). P1 was previously shown to draw water to the bilayer.[50]

(*d*: bilayer thickness, including associated water layer) and the bilayer electron density profiles when the plain lipids are exposed to SL-HE or SL-HE/P1 at L/P = 20:1 and P/SL-HE = 1:8.

There is a dramatic decrease, by 4 Å, in the repeat spacing upon incorporation of SL-HE into the POPC/POPG bilayer (Figure 11A). This is accompanied by a 2.7 Å decrease in the

phosphate-to-phosphate distance (Figure 11B), providing strong evidence that the glycolipid is incorporated into the phospholipids and causes thinning of the bilayer. The increase in electron density around the bilayer surfaces for the SL-HE/POPC/POPG sample compared to neat POPC/POPG is most likely due to sugar groups projecting at the bilayer surface and causing additional water accumulation. Furthermore, the loss of structural details in the hydrocarbon region (Figure 11B) in the presence of SL-HE indicates that the glycolipid hydrocarbon tails induce disorder in the hydrocarbon core. Such effects on the bilayer structure are similar to those observed for nonionic detergents and associated with an increase in the lateral area per lipid upon incorporation of the carbohydrate-based amphiphile into the phospholipid bilayer.[122]

When P1 is added to the SL-HE/POPC/POPG mixture, it causes a further dramatic decrease in the repeat spacing by almost 3 Å (for a total of ~7 Å compared to neat POPC/POPG), accompanied by a "peak splitting" in the Bragg diffraction pattern. This is different from the effects we previously observed for P1 alone added to 3:1 POPC/POPG bilayers,[50] where the reduction in *d* did not exceed 3.5 Å upon P1 incorporation, for an equivalent L/P of 20:1. While it is not clear whether the peptide binds preferentially to the glycolipid component or any of the two phospholipids, the split peaks indicate the presence of at least two separated phases both with repeat spacings smaller than the SL-HE/POPC/POPG sample without peptide. This indicates that P1 causes segregation in such a complex mixture by favoring one of the components. By concentrating itself in one region of the bilayer, it can more readily reach the threshold concentration needed to disrupt the membrane.

Overall, these XRD data describe for the first time the response of a phospholipid bilayer to an SL-ester alone and in combination with a membrane-active peptide. Strikingly, phase separation occurs when both the glycolipid and the peptide are present. Such a phase separation, as revealed by XRD, is a crucial finding since it provides a mechanistic basis to explain the stronger membrane disruption and permeabilization that can be achieved when P1/3 is associated with SL-HE. First, both the SL-HE and piscidin peptides have the ability to thin and disorder the bilayer, with each agent being able to leverage the defects formed by the other. Second, the unique ability of piscidin to preferentially associate with some lipids in the mixture triggers phase separation in the membrane, enhancing the ability of the peptide to reach a critical concentration for membrane disruption.

DISCUSSION

The cosecretion of multiple antimicrobial agents is a feature commonly evolved in multicellular organisms to fight pathogenic bacteria.[6−14] In this research, we investigated the synergy of two families of naturally produced antimicrobials to better address a growing number of bacteria that resist conventional treatment options. Our selection includes P1 and P3, membrane-active HDPs potent on drug-resistant bacteria,[43,44,51] and the glycolipid SL-HE, a modified product from nonpathogenic yeast fermentation.[56] SLs feature attractive features for drug development, including safe biocompatibility profiles and low production costs.[58,65] While many SL structures exhibit antimicrobial activity, SL-HE used at 200 μM is inactive on the bacteria strains *S. aureus* (ATCC 33807), *B. cereus* (ATCC 4342), *B. subtilis* (ATCC 21332), *L. innocua* (ATCC 33090), and *E. coli* (ATCC 53323).[64] We hypothesized that,

given the amphipathic nature of SL-HE and P1/3, combining them would facilitate their simultaneous colocalization with membranes, ultimately potentiating synergistic action on bacteria. Our experiments with the pathogenic strain *B. cereus* (ATCC 4342) validate this hypothesis and show that the synergy is accompanied by enhanced membrane permeabilization. Utilizing complementary biophysical methods, we demonstrate that SL-HE is membrane active. Its synergistic effect with piscidin is underpinned by the formation of peptide/SL-HE complexes that enable the two agents to coordinate their membrane activity spatially and temporally. Below, we discuss these results and highlight their significance and implications, especially regarding the development of novel antimicrobial therapeutics to fight drug-resistant bacteria.

As part of the testing for enhanced efficiency by the two-drug combination featuring SL-HE and P1/3, a checkerboard experiment in a 96-multiwell-plate was performed. P/SL covered a range from 1:64 to 128:1. Even though SL-HE is inactive alone, it synergized with P1/3. Thus, SL-HE has intrinsic chemical features (e.g., hydrophobic character; micellar organization) that can be leveraged to elicit synergistic effects. Based on the results in Figure 2, the lowest concentration of piscidin needed to synergistically inhibit bacterial growth in the presence of SL-HE is [P1/3] = 0.5 μM and [SL-HE] = 8 and 16 μM. For P1 and P3 that have respective MICs of 2 and 4 μM, this corresponds to a 4- and 8-fold improvement in activity, respectively. Notably, this enables P3 to become as effective as P1 when it is combined with SL-HE. If we consider the improvement from the perspective of SL-HE, the lowest concentration of SL-HE that is synergistically inhibitory with piscidin occurs at [SL-HE] = 2 μM and [P1] = 1 μM. Since the MIC for SL-HE is >200 μM,[64] this corresponds to an improvement of at least 100-fold under conditions where the peptide concentration is used at half of its MIC. With a submicromolar concentration of P1/3 (0.5 μM), 8 μM SL-HE is inhibitory, translating into an enhancement in potency greater than 25-fold. From a drug development standpoint, such combinations where the peptide concentration is ≤1 μM are highly beneficial since peptides are more expensive to produce than SLs and tend to have narrower therapeutic windows. Here, we can estimate the therapeutic index (TI) of the peptide/SL combination. Taking P1 as an example in the mixture where it is used at 0.5 μM and SL-HE = 8 μM and using the previously published IC$_{50}$ value of >10 μM for P1 on human primary gingival fibroblast and oral mucosal fibroblast cells[123] and >200 μM for SL-HE on macrophages,[124] we find that the TI value is >20 for P1 and >25 for SL-HE. Drugs with TI values >10 are typically assumed to be safe.[125] To build on these promising results from biological assays, biophysical studies were conducted to understand the mechanism underlying the synergy of these two agents.

As a surfactant, SL-HE forms micelles in solution. NMR and CD experiments show that P1/3 bind to these micelles.[67,69] The SL micellar behavior shows little change upon peptide binding, albeit slower diffusion is observed by DOSY NMR. Both P1 and P3 were previously found to interact with detergent micelles (e.g., sodium dodecyl sulfate (SDS) and dodecylphosphocho-line (DPC)) and bicelles.[50,99,126] Given the similar amphipathic nature of the SL-HE, DPC, and SDS molecules, we speculate that piscidin binds to the surface of the micelles and buries its hydrophobic side chains in the nonpolar region of micelles where the acyl tails of the glycolipid reside.[50]

Our CD experiments provide definitive evidence that SL-HE micelles binding to the peptide induce a conformational change from random coil to an α-helix. To determine the dissociation constants, K_d, between the peptide and SL, data correlating SL-HE concentration and piscidin helicity were fitted to a bimolecular binding equation. Values of K_d range from about 200 to 400 μM for SL-HE binding with P1 and P3, respectively. In prior work with 3:1 POPC/POPG and in the absence of SL-HE as bacterial cell membrane mimics, the K_d was about 100 μM for both P1 and P3.[78] Since the dissociation constant is smaller when the peptides interact with the phospholipids than the SL-HE micelles, the peptide has a stronger affinity for the former, explaining why the peptide transfers to membranes when SL/piscidin complexes are exposed to phospholipid bilayers.

Importantly, in the presence of phospholipid bilayers, MS, NMR, and XRD data show that SL-HE micelles do not remain intact, since the membrane becomes enriched in SL molecules. According to the XRD results, the incorporation of SL in the membrane is accompanied by a strong disruption of the bilayer structure, regardless of whether the peptide is present or not. Consequently, membrane activity is an intrinsic property of SL-HE. This is important since direct evidence to show that SLs can integrate into and disrupt phospholipid membranes was previously lacking.

While the exact molecular arrangement of the peptide, SL-HE, and phospholipids has not yet been established, several important mechanistic features emerge from the biophysical studies conducted herein regarding the mechanism by which piscidin and SL-HE synergistically disrupt membranes. First, CD and NMR studies reveal that the glycolipid micelles provide an environment conducive to peptide binding and folding into an α-helix, which is the state adopted by the peptide when it binds to and disrupts membranes. The entropy cost of folding the peptide into a secondary structure would be compensated when the peptide binds to the SL micelles and buries its hydrophobic side chains within the nonpolar region of the micelles. Consequently, the peptide prebound to the SL-HE micelles is structurally primed before it encounters bacterial membranes.

Second, SPR experiments highlight that the peptide and SL-HE function cooperatively to reach membranes. Specifically, when the peptide and SL-HE are added together, and thus coalesced both spatially and temporally, a massive accumulation of material onto membranes is evident by SPR. Importantly, this large delivery of materials does not occur in the absence of either the peptide or SL-HE. Since piscidin, as a cationic agent, very likely coats the surface of the SL-HE micelles, a strong electrostatic interaction is possible between the SL-HE/peptide complex and the negative surface of the membrane. This could, in part, explain the strong accumulation observed by SPR. This also suggests that the physical association of SL micelles and HDPs in a way that places the cationic peptides on the surface of the SL micelles represents an important strategy to target antimicrobial agents to the vital plasma membrane of pathogens.

Third, while the peptide and glycolipid are individually able to disrupt membranes, the integration of both in the membrane produces a dramatic structural rearrangement of the membrane, as shown by XRD. The decrease in the bilayer thickness, which surpasses any such effects for the peptides alone under the same measurement conditions,[49,50,53] is consistent with the presence of SL-HE and piscidin in the membrane, in agreement with the MS (SL-HE signal in Figure 5) and solid-state NMR (piscidin signal in Figure 10) data. Based on the SPR data described

above, flowing both SL-HE and piscidin onto the membrane produces a cooperative mass increase. This can happen if the SL-HE carbohydrate groups act as peptide "recruiter" that boost peptide transfer and accumulation to a bilayer interface already disrupted by the incorporation of SL-HE. Furthermore, in previous studies featuring PC/cholesterol to mimic mammalian cell membranes,[49] P1 and P3 were found to induce domain separation in membranes such that they partitioned into a more disordered, fluid phase by expelling cholesterol from the area where it was bound, thereby causing domain segregation. Here, SL-HE incorporation into PC/PG lipid bilayers possibly has a similar disordering effect in the sample containing piscidin with domain separation occurring. As described by the SMART (Soft Membranes Adapt and Respond, also Transiently) model, the addition of membrane-active substances, such as amphipathic peptides and surfactants, can induce changes in the phase diagrams of phospholipids and promote the formation of disrupted states, including nonbilayer structures.[121] Here, differing binding affinities of P1 for the various bilayer components (PC, PG, and SL-HE) could be the cause of the domain separation in the P1/POPC/POPG/SL-HE bilayers. Given its sensitivity to lipid polymorphism, ^{31}P NMR on whole vesicles could be useful to further characterize the disrupted state detected by XRD.[127−131] Altogether, the presence of SL-HE exacerbates membrane disruption by piscidin as SL-HE recruits more peptide to the membrane, contributes to phase separation, as shown by the split peaks in Figure 11, and forms membrane defects that piscidin can leverage. These combined effects of piscidin and SL-HE help explain the dramatic bilayer thinning, synergistic mass increase, and enhanced membrane leakage observed by XRD, SPR, and permeabilization assays.

Piscidins are active on a broad range of pathogens as well as cancer cells. The involvement of sugar groups in the recruitment role of SL-HE is relevant for both pathogenic and cancer cells, which are all enriched in carbohydrates.[132] While piscidins bind to various types of bilayer membranes (model and natural membranes), both P1/3 peptides bind strongly to LPS,[52] characteristic of Gram-negative bacterial cell walls and to various types of mammalian cancer cells,[53,123,133] which are also rich in carbohydrates.[132]

While we are not aware of other reports where SLs and HDPs were synergized against bacteria, a few other studies highlight the synergistic effects between HDPs and rhamnolipids, which are glycolipids derived from *Pseudomonas aeruginosa* (*P. aeruginosa*).[134−136] Similar to SLs, rhamnolipids belong to the family of glycolipid biosurfactants. They contain a rhamnose ring and a lipid component consisting of at least one fatty acid chain. They can have antitumor, antifungal, antibacterial, and antibiofilm activity while remaining safe.[134−136] Whereas the mechanism of action of rhamnolipids on bacterial cells is not known, they are believed to be membrane disruptive due to their amphipathic structures that are conducive to membrane insertion.[137] Sana et al. investigated the combination of two biosurfactants, a lipopeptide BS15 and a rhamnolipid from *P. aeruginosa* on *S. aureus* and *E. coli*.[138] Synergy was observed between the two agents. Through SEM imaging of bacterial cells, leakage of protein content, and crystal violet to measure the alteration of membrane permeability, it was concluded that membrane disruption was occurring in the presence of the synergistic combination. Magalhães and Nitschke studied the combination of the antimicrobial peptide nisin with rhamnolipids.[139] The study was motivated by the fact that both nisin and rhamnolipids are used in food products. Nisin is used as an

antimicrobial substance against Gram-positive bacteria found in foods such as *Listeria monocytogenes*, and rhamnolipids have emulsifying properties. Nisin can form pores in the membranes of cells it targets. The authors found synergy, with an FIC index as low as 0.078 for some combinations. They speculated that the negative carboxylic acid charge of rhamnolipids at physiological pH and their ability to partition into membranes could elicit the same type of membrane changes that Tween 20 does as an anionic surfactant, leading bacteria to increase their membrane content of negative lipids to repel the exogenous agent. Hence, nisin, which is cationic, would be able to interact more readily with these membranes. While these studies with rhamnolipids point at a mechanism of action that targets cell membranes, the mechanism of action for the synergy remains uncharacterized on a molecular level.

Future improvements in the biological activity of peptide-glycolipid dual component systems depend on a deeper understanding of the mechanisms of action on a molecular level. Given the similarities between SLs and rhamnolipids, our work could help us better understand how other naturally derived glycolipids, such as rhamnolipids, achieve their function when they are combined with peptides. It is important to note that our investigations with model membranes do not explore an additional level of synergy where the antimicrobial agents would not only disrupt microbial membranes but also gain access to intracellular targets.

In vivo, host defense mechanisms feature the cosecretion of antimicrobial agents,[6−14] but few examples exist that document the physical association of the agents with each other, a key feature demonstrated here for P1/3 and SL-HE. However, there are some notable examples. A previous study by our team reported that piscidin has a metal binding motif that enables the peptide to bind to Cu^{2+},[46,140,141] which is found in phagosomes and has antimicrobial activity due to its redox character.[14] Cu^{2+}-binding enhances significantly the antimicrobial and anticancer activities of P1 and P3.[46,53,78] It has also been found that the two HDPs, magainin and PLGa, interact with membranes in a way that stabilizes the insertion of PLGa in a transmembrane orientation, an effect that correlates with synergistic effects on bacteria.[142,143]

Physical association between two antimicrobial agents represents an advantage if it can be maintained *in vivo* to ensure that the compounds can exert concerted action spatially and temporally. Given that the peptide dissociates from SL-HE micelles, it would be necessary for the assembly to be engineered in such a way that it remains associated. This would allow the P1/3-SL-HE aggregate to maintain enhanced activity at the site of an infection. By developing environments where the association of aggregates can be maintained, we could leverage the remarkable opportunity where a synergistic binary combination makes it possible to use less of the agent that is more expensive and has a narrower therapeutic window, while the low-cost and highly biocompatible agent, which is inactive on its own, lends a useful peptide-recruiter role. Based on these preliminary studies, piscidin/SL combinations could become promising candidates for topical treatments since ointments directly act at the site of applications.

■ CONCLUSION

All kingdoms of life rely on HDPs as part of their first line of immune defense. SLs, which are produced by a selected group of organisms, exhibit highly advantageous properties, including strong biocompatibility, low production cost, and beneficial

biological activity, including antimicrobial effects. This study highlights promising synergistic antimicrobial action obtained by mixing an inactive SL with HDPs P1 and P3. Combining SL-HE with subinhibitory concentrations of P1/P3 enables increases in antimicrobial activity against *B. cereus* of greater than 2 orders of magnitude, enabling a clear reduction of the dosage needed for antimicrobial action and likely important improvements in the therapeutic window. Despite its low antimicrobial activity on microorganisms cited above, SL-HE integrates into bilayers and exhibits membrane activity, features that were previously unknown. Mechanistic characterization demonstrates a novel strategy in which bacterial cell death can be more effectively achieved by forming a macromolecular assembly between P1/3 and SL-HE, so that the entire payload is delivered at once. The carbohydrate group could be involved in the binding, insertion, and accumulation of HDP into the membrane, enhancing the interactions and disruptive effects of the peptides on cells. Overall, the SL-HE micelles perform multiple functions of promoting the active state of the peptide, concentrating it locally, relieving the entropy cost associated with peptide folding as it binds to phospholipid bilayers, and helping to recruit the peptide to phospholipid membranes. Furthermore, SL-HE integrates into membranes, inducing membrane disruption that HDP can leverage. Since SLs are already safely employed in consumer products and SL/piscidin complexes target membranes, the combinations designed and the mechanistic investigations disclosed in this study provide fertile ground to develop novel strategies to fight drug-resistant bacteria.

■ ASSOCIATED CONTENT

ⓢ Supporting Information

The Supporting Information is available free of charge at https://pubs.acs.org/doi/10.1021/jacsau.3c00506.

> Figures showing the permeabilization effects of SL-HE on 3:1 POPC/POPG vesicles; MS data collected on phospholipid bilayers exposed to the glycolipid and peptide; plots of kinetics parameters obtained from SPR (PDF)

■ AUTHOR INFORMATION

Corresponding Authors

Myriam L. Cotten − *Department of Applied Science, William & Mary, Williamsburg, Virginia 23185, United States;* ⓞ orcid.org/0000-0002-6732-1736; Email: mcotten@wm.edu; Fax: (757)-221-2050

Richard Gross − *Department of Chemistry and Center for Biotechnology and Interdisciplinary Studies, Rensselaer Polytechnic Institute, Troy, New York 12180, United States;* ⓞ orcid.org/0000-0002-5050-3162; Email: grossr@rpi.edu; Fax: (518)-276-3405

Authors

Fei Liu − *Department of Chemistry, Rensselaer Polytechnic Institute, Troy, New York 12180, United States*

Alexander I. Greenwood − *Department of Applied Science, William & Mary, Williamsburg, Virginia 23185, United States*

Yawei Xiong − *Department of Applied Science, William & Mary, Williamsburg, Virginia 23185, United States*

Rebecca T. Miceli − *Department of Chemistry and Center for Biotechnology and Interdisciplinary Studies, Rensselaer*

Polytechnic Institute, Troy, New York 12180, United States; ⓞ orcid.org/0000-0002-2297-9219

Riqiang Fu − *Center of Interdisciplinary Magnetic Resonance, National High Magnetic Field Laboratory, Tallahassee, Florida 32310, United States;* ⓞ orcid.org/0000-0003-0075-0410

Kyle W. Anderson − *National Institute of Standards and Technology, Rockville, Maryland 20850, United States;* ⓞ orcid.org/0000-0002-2808-3026

Scott A. McCallum − *Center for Biotechnology and Interdisciplinary Studies, Rensselaer Polytechnic Institute, Troy, New York 12180, United States*

Mihaela Mihailescu − *Institute for Bioscience and Biotechnology Research, University of Maryland, Rockville, Maryland 20850, United States*

Complete contact information is available at:
https://pubs.acs.org/10.1021/jacsau.3c00506

Author Contributions

M.L.C. and R.G. conceptualized the overall synergy project. The biological assays and SPR experiments were designed and performed by F.L. and M.L.C. The calcein leakage assay was planned by M.L.C. and Y.X. and performed by Y.X. The CD experiments were designed and performed by M.L.C with A.I.G. fitting the data. S.A.M., R.T.M., and M.L.C. designed the solution NMR experiments with S.A.M. and R.T.M. carrying out the experiments. The solid-state NMR experiments were planned by M.L.C., and the samples were made by M.L.C.; M.L.C., A.I.G., and R.F. performed the solid-state NMR experiments. M.L.C. and M.M. planned the samples for XRD and EIS-MS with Y.X. helping to make the samples. M.M. and K.W.A. performed the XRD and EIS-MS experiments. The full draft of the manuscript was prepared and refined by M.L.C. with some text and figure materials for specific sections coming from coauthors. M.L.C. made the TOC graphic. All coauthors provided feedback on the manuscript. CRediT: **Fei Liu** data curation, formal analysis, investigation, methodology, visualization, writing-review & editing; **Alexander I. Greenwood** formal analysis, investigation, methodology, validation, visualization, writing-review & editing; **Yawei Xiong** data curation, formal analysis, investigation, visualization, writing-review & editing; **Rebecca T Miceli** data curation, formal analysis, investigation, visualization, writing-review & editing; **Riqiang Fu** data curation, formal analysis, methodology, resources, writing-review & editing; **Kyle W. Anderson** data curation, formal analysis, investigation, methodology, resources, visualization, writing-review & editing; **Scott A McCallum** conceptualization, data curation, formal analysis, investigation, methodology, resources, supervision, validation, visualization, writing-review & editing; **Mihaela Mihailescu** conceptualization, data curation, formal analysis, funding acquisition, investigation, methodology, resources, supervision, validation, visualization, writing-review & editing; **Richard A Gross** conceptualization, data curation, formal analysis, funding acquisition, investigation, methodology, project administration, resources, supervision, validation, writing-review & editing; **Myriam L. Cotten** conceptualization, data curation, formal analysis, funding acquisition, investigation, methodology, project administration, resources, software, supervision, validation, visualization, writing-original draft, writing-review & editing.

Notes

The authors declare no competing financial interest.

■ ABBREVIATIONS

APD: Antimicrobial Peptide Database; *B. cereus*: *Bacillus cereus*; *B. subtilis*: *Bacillus subtilis*; *S. aureus*: *Staphylococcus aureus*; *L. innocua*: *Listeria innocua*; CHAPS: 3-[(3-cholamidopropyl)-dimethylammonio]-1-propanesulfonate; CD: circular dichroism; CMC: critical micellar concentration; DMPC: dimyristoyl-*sn*-glycero-3-phosphocholine; DMPG: 1,2-dimyristoyl-*sn*-glycero-3-phosphoglycerol; DOSY: diffusion-ordered spectroscopy; DPC: dodecylphosphocholine; *E. coli*: *Escherichia coli*; EIS-MS: electrospray ionization mass spectrometry; HPLC: high performance liquid chromatography; HDP: host defense peptide; FIC: fractional inhibitory concentration; LUV: large unilamellar vesicle; L/P: lipid-to-peptide molar ratio; MS: mass spectrometry; MIC: minimum inhibitory concentration; MHB: Mueller-Hinton broth; PBS: phosphate-buffered saline; P1: piscidin 1; P3: piscidin 3; P/SL-HE: peptide-to-sophorolipid molar ratio; OS SS-NMR: oriented sample solid-state NMR; POPC: 1-palmitoyl-2-oleoyl-*sn*-glycero-3-phosphocholine; POPG: 1-palmitoyl-2-oleoyl-*sn*-glycero-3-phosphoglycerol; RU: response unit; SDS: sodium dodecyl sulfate; SEM: scanning electron microscope; SL: sophorolipid; SB-BE: sophorolipid-butyl ester; SL-HE: sophorolipid-hexyl ester; SPR: surface plasmon resonance; SLB: supported lipid bilayer; TI: therapeutic index; TSB: tryptic soy broth

■ REFERENCES

(1) Baym, M.; Stone, L. K.; Kishony, R. Multidrug evolutionary strategies to reverse antibiotic resistance. *Science* **2016**, *351*, 1147−1151.

(2) Karam, G.; Chastre, J.; Wilcox, M. H.; Vincent, J. L. Antibiotic strategies in the era of multidrug resistance. *Crit Care* **2016**, *20*, 136.

(3) Munita, J. M.; Arias, C. A. Mechanisms of Antibiotic Resistance. *Microbiol Spectr* **2016**, *4*, 1.

(4) Lesho, E. P.; Laguio-Vila, M. The Slow-Motion Catastrophe of Antimicrobial Resistance and Practical Interventions for All Prescribers. *Mayo Clin Proc.* **2019**, *94*, 1040−1047.

(5) Ribeiro da Cunha, B.; Fonseca, L. P.; Calado, C. R. C. Antibiotic Discovery: Where Have We Come from, Where Do We Go? *Antibiotics (Basel, Switzerland)* **2019**, *8*, 45.

(6) Greve, J. M.; Cowan, J. A. Tackling antimicrobial stewardship through synergy and antimicrobial peptides. *RSC Med. Chem.* **2022**, *13*, 511−521.

(7) Hanson, M. A.; Dostálová, A.; Ceroni, C.; Poidevin, M.; Kondo, S.; Lemaitre, B. Synergy and remarkable specificity of antimicrobial peptides in vivo using a systematic knockout approach. *eLife* **2019**, *8*, No. e44341.

(8) Doolin, T.; Amir, H. M.; Duong, L.; Rosenzweig, R.; Urban, L. A.; Bosch, M.; Pol, A.; Gross, S. P.; Siryaporn, A. Mammalian histones facilitate antimicrobial synergy by disrupting the bacterial proton gradient and chromosome organization. *Nat. Commun.* **2020**, *11*, 3888.

(9) Abou Alaiwa, M. H.; Reznikov, L. R.; Gansemer, N. D.; Sheets, K. A.; Horswill, A. R.; Stoltz, D. A.; Zabner, J.; Welsh, M. J. pH modulates the activity and synergism of the airway surface liquid antimicrobials β-defensin-3 and LL-37. *Proc. Natl. Acad. Sci. U. S. A.* **2014**, *111*, 18703−8.

(10) Duong, L.; Gross, S. P.; Siryaporn, A. Developing Antimicrobial Synergy With AMPs. *Front Med. Technol.* **2021**, *3*, 640981.

(11) Howell, M.; Wenc, A. K.; Donaghy, C. M.; Wasche, D. V.; Abissi, I.; Naing, M. D.; Pierce, S.; Angeles-Boza, A. M. Exploring synergy and its role in antimicrobial peptide biology. *Methods Enzymol* **2022**, *663*, 99−130.

(12) Drake, D. R.; Brogden, K. A.; Dawson, D. V.; Wertz, P. W. Thematic Review Series: Skin Lipids. Antimicrobial lipids at the skin surface. *J. Lipid Res.* **2008**, *49*, 4−11.

(13) Brogden, K. A.; Guthmiller, J. M.; Salzet, M.; Zasloff, M. The nervous system and innate immunity: the neuropeptide connection. *Nat. Immunol.* **2005**, *6*, 558−64.

(14) Besold, A. N.; Culbertson, E. M.; Culotta, V. C. The Yin and Yang of copper during infection. *J. Biol. Inorg. Chem.* **2016**, *21*, 137−44.

(15) Blyth, G. A. D.; Connors, L.; Fodor, C.; Cobo, E. R. The Network of Colonic Host Defense Peptides as an Innate Immune Defense Against Enteropathogenic Bacteria. *Front Immunol* **2020**, *11*, 965−965.

(16) Mansour, S. C.; de la Fuente-Nunez, C.; Hancock, R. E. Peptide IDR-1018: modulating the immune system and targeting bacterial biofilms to treat antibiotic-resistant bacterial infections. *J. Pept Sci.* **2015**, *21*, 323−9.

(17) Anantharaman, A.; Rizvi, M. S.; Sahal, D. Synergy with rifampin and kanamycin enhances potency, kill kinetics, and selectivity of de novo-designed antimicrobial peptides. *Antimicrob. Agents Chemother.* **2010**, *54*, 1693−9.

(18) Wu, X.; Li, Z.; Li, X.; Tian, Y.; Fan, Y.; Yu, C.; Zhou, B.; Liu, Y.; Xiang, R.; Yang, L. Synergistic effects of antimicrobial peptide DP7 combined with antibiotics against multidrug-resistant bacteria. *Drug Des Devel Ther* **2017**, *11*, 939−946.

(19) Li, J.; Fernández-Millán, P.; Boix, E. Synergism between Host Defence Peptides and Antibiotics Against Bacterial Infections. *Curr. Top Med. Chem.* **2020**, *20*, 1238−1263.

(20) Xia, Y.; Cebrián, R.; Xu, C.; Jong, A.; Wu, W.; Kuipers, O. P. Elucidating the mechanism by which synthetic helper peptides sensitize Pseudomonas aeruginosa to multiple antibiotics. *PLoS Pathog* **2021**, *17*, No. e1009909.

(21) Zhu, Y.; Hao, W.; Wang, X.; Ouyang, J.; Deng, X.; Yu, H.; Wang, Y. Antimicrobial peptides, conventional antibiotics, and their synergistic utility for the treatment of drug-resistant infections. *Med. Res. Rev.* **2022**, *42*, 1377−1422.

(22) McCafferty, D. G.; Cudic, P.; Yu, M. K.; Behenna, D. C.; Kruger, R. Synergy and duality in peptide antibiotic mechanisms. *Curr. Opin Chem. Biol.* **1999**, *3*, 672−80.

(23) Bolosov, I. A.; Kalashnikov, A. A.; Panteleev, P. V.; Ovchinnikova, T. V. Analysis of Synergistic Effects of Antimicrobial Peptide Arenicin-1 and Conventional Antibiotics. *Bull. Exp. Biol. Med.* **2017**, *162*, 765−768.

(24) Ruden, S.; Rieder, A.; Chis Ster, I.; Schwartz, T.; Mikut, R.; Hilpert, K. Synergy Pattern of Short Cationic Antimicrobial Peptides Against Multidrug-Resistant Pseudomonas aeruginosa. *Front. Microbiol.* **2019**, *10*, 2740.

(25) Li, D.; Yang, Y.; Tian, Z.; Lv, J.; Sun, F.; Wang, Q.; Liu, Y.; Xia, P. Synergistic antibiotic effect of looped antimicrobial peptide CLP-19 with bactericidal and bacteriostatic agents. *Oncotarget* **2017**, *8*, 55958−55966.

(26) Kampshoff, F.; Willcox, M. D. P.; Dutta, D. A Pilot Study of the Synergy between Two Antimicrobial Peptides and Two Common Antibiotics. *Antibiotics* **2019**, *8*, 60.

(27) Sheard, D. E.; O'Brien-Simpson, N. M.; Wade, J. D.; Separovic, F. Combating bacterial resistance by combination of antibiotics with antimicrobial peptides. *Pure Appl. Chem.* **2019**, *91*, 199−209.

(28) Mansour, S. C.; Pena, O. M.; Hancock, R. E. Host defense peptides: front-line immunomodulators. *Trends Immunol.* **2014**, *35*, 443−50.

(29) Haney, E. F.; Hancock, R. E. W. Peptide design for antimicrobial and immunomodulatory applications. *Biopolymers* **2013**, *100*, 572−583.

(30) Hancock, R. E.; Nijnik, A.; Philpott, D. J. Modulating immunity as a therapy for bacterial infections. *Nat. Rev. Microbiol.* **2012**, *10*, 243−54.

(31) Magana, M.; Pushpanathan, M.; Santos, A. L.; Leanse, L.; Fernandez, M.; Ioannidis, A.; Giulianotti, M. A.; Apidianakis, Y.; Bradfute, S.; Ferguson, A. L.; Cherkasov, A.; Seleem, M. N.; Pinilla, C.; de la Fuente-Nunez, C.; Lazaridis, T.; Dai, T.; Houghten, R. A.; Hancock, R. E. W.; Tegos, G. P. The value of antimicrobial peptides in the age of resistance. *Lancet Infect. Dis.* **2020**, *20*, e216−e230.

(32) Mookherjee, N.; Anderson, M. A.; Haagsman, H. P.; Davidson, D. J. Antimicrobial host defence peptides: functions and clinical potential. *Nat. Rev. Drug Disc.* **2020**, *19*, 311−332.

(33) van Dijk, A.; Hedegaard, C. J.; Haagsman, H. P.; Heegaard, P. M. H. The potential for immunoglobulins and host defense peptides (HDPs) to reduce the use of antibiotics in animal production. *Vet Res.* **2018**, *49*, 68.

(34) Kintses, B.; Méhi, O.; Ari, E.; Számel, M.; Györkei, Á.; Jangir, P. K.; Nagy, I.; Pál, F.; Fekete, G.; Tengölics, R.; Nyerges, Á.; Likó, I.; Bálint, A.; Molnár, T.; Bálint, B.; Vásárhelyi, B. M.; Bustamante, M.; Papp, B.; Pál, C. Phylogenetic barriers to horizontal transfer of antimicrobial peptide resistance genes in the human gut microbiota. *Nat. Microbiol.* **2019**, *4*, 447−458.

(35) Peschel, A.; Sahl, H. G. The co-evolution of host cationic antimicrobial peptides and microbial resistance. *Nat. Rev. Microbiol.* **2006**, *4*, 529−36.

(36) Kong, Q.; Six, D. A.; Liu, Q.; Gu, L.; Wang, S.; Alamuri, P.; Raetz, C. R. H.; Curtiss, R., 3rd Phosphate groups of lipid A are essential for Salmonella enterica serovar Typhimurium virulence and affect innate and adaptive immunity. *Infect. Immun.* **2012**, *80*, 3215−3224.

(37) Izoré, T.; Tailhades, J.; Hansen, M. H.; Kaczmarski, J. A.; Jackson, C. J.; Cryle, M. J. *Drosophila melanogaster* nonribosomal peptide synthetase Ebony encodes an atypical condensation domain. *Proc. Natl. Acad. Sci. U. S. A.* **2019**, *116*, 2913.

(38) Rea, M. C.; Sit, C. S.; Clayton, E.; O'Connor, P. M.; Whittal, R. M.; Zheng, J.; Vederas, J. C.; Ross, R. P.; Hill, C. Thuricin CD, a posttranslationally modified bacteriocin with a narrow spectrum of activity against *Clostridium difficile. Proc. Natl. Acad. Sci. U. S. A.* **2010**, *107*, 9352.

(39) Pérez-Cobas, A. E.; Moya, A.; Gosalbes, M. J.; Latorre, A. Colonization Resistance of the Gut Microbiota against Clostridium difficile. *Antibiotics (Basel)* **2015**, *4*, 337−57.

(40) Silveira, G. G. O. S.; Torres, M. D. T.; Ribeiro, C. F. A.; Meneguetti, B. T.; Carvalho, C. M. E.; de la Fuente-Nunez, C.; Franco, O. L.; Cardoso, M. H. Antibiofilm Peptides: Relevant Preclinical Animal Infection Models and Translational Potential. *ACS Pharmacol. Transl. Sci.* **2021**, *4*, 55−73.

(41) Torres, M. D. T.; Cao, J.; Franco, O. L.; Lu, T. K.; de la Fuente-Nunez, C. Synthetic Biology and Computer-Based Frameworks for Antimicrobial Peptide Discovery. *ACS Nano* **2021**, *15*, 2143−2164.

(42) Wang, G.; Li, X.; Wang, Z. APD2: the updated antimicrobial peptide database and its application in peptide design. *Nucleic Acids Res.* **2009**, *37*, D933−7.

(43) Lauth, X.; Shike, H.; Burns, J. C.; Westerman, M. E.; Ostland, V. E.; Carlberg, J. M.; Van Olst, J. C.; Nizet, V.; Taylor, S. W.; Shimizu, C.; et al. Discovery and characterization of two isoforms of moronecidin, a novel antimicrobial peptide from hybrid striped bass. *J. Biol. Chem.* **2002**, *277*, 5030−5039.

(44) Silphaduang, U.; Noga, E. J. Peptide antibiotics in mast cells of fish. *Nature* **2001**, *414*, 268−269.

(45) Chekmenev, E. Y.; Vollmar, B. S.; Forseth, K. T.; Manion, M. N.; Jones, S. M.; Wagner, T. J.; Endicott, R. M.; Kyriss, B. P.; Homem, L. M.; Pate, M.; He, J.; Raines, J.; Gor'kov, P. L.; Brey, W. W.; Mitchell, D. J.; Auman, A. J.; Ellard-Ivey, M.; Blazyk, J.; Cotten, M. Investigating molecular recognition and biological function at interfaces using piscidins, antimicrobial peptides from fish. *Biochim. Biophys. Acta* **2006**, *1758*, 1359−1372.

(46) Libardo, M. D. J.; Bahar, A. A.; Ma, B.; Fu, R.; McCormick, L. E.; Zhao, J.; McCallum, S. A.; Nussinov, R.; Ren, D.; Angeles-Boza, A. M.; Cotten, M. L. Nuclease activity gives an edge to host-defense peptide piscidin 3 over piscidin 1, rendering it more effective against persisters and biofilms. *FEBS J.* **2017**, *284*, 3662−3683.

(47) Hayden, R. M.; Goldberg, G. K.; Ferguson, B. M.; Schoeneck, M. W.; Libardo, M. D.; Mayeux, S. E.; Shrestha, A.; Bogardus, K. A.; Hammer, J.; Pryshchep, S.; Lehman, H. K.; McCormick, M. L.; Blazyk, J.; Angeles-Boza, A. M.; Fu, R.; Cotten, M. L. Complementary Effects of Host Defense Peptides Piscidin 1 and Piscidin 3 on DNA and Lipid Membranes: Biophysical Insights into Contrasting Biological Activities. *J. Phys. Chem. B* **2015**, *119*, 15235−46.

(48) Kim, S. Y.; Zhang, F.; Gong, W.; Chen, K.; Xia, K.; Liu, F.; Gross, R.; Wang, J. M.; Linhardt, R. J.; Cotten, M. L. Copper regulates the interactions of antimicrobial piscidin peptides from fish mast cells with formyl peptide receptors and heparin. *J. Biol. Chem.* **2018**, *293*, 15381−15396.

(49) Comert, F.; Greenwood, A.; Maramba, J.; Acevedo, R.; Lucas, L.; Kulasinghe, T.; Cairns, L. S.; Wen, Y.; Fu, R.; Hammer, J.; Blazyk, J.; Sukharev, S.; Cotten, M. L.; Mihailescu, M. The host-defense peptide piscidin P1 reorganizes lipid domains in membranes and decreases activation energies in mechanosensitive ion channels. *J. Biol. Chem.* **2019**, *294*, 18557−18570.

(50) Mihailescu, M.; Sorci, M.; Seckute, J.; Silin, V. I.; Hammer, J.; Perrin, B. S., Jr; Hernandez, J. I.; Smajic, N.; Shrestha, A.; Bogardus, K. A.; Greenwood, A. I.; Fu, R.; Blazyk, J.; Pastor, R. W.; Nicholson, L. K.; Belfort, G.; Cotten, M. L. Structure and Function in Antimicrobial Piscidins: Histidine Position, Directionality of Membrane Insertion, and pH-Dependent Permeabilization. *J. Am. Chem. Soc.* **2019**, *141*, 9837−9853.

(51) Oludiran, A.; Courson, D. S.; Stuart, M. D.; Radwan, A. R.; Poutsma, J. C.; Cotten, M. L.; Purcell, E. B. How Oxygen Availability Affects the Antimicrobial Efficacy of Host Defense Peptides: Lessons Learned from Studying the Copper-Binding Peptides Piscidins 1 and 3. *Int. J. Mol. Sci.* **2019**, *20*, 5289.

(52) Cetuk, H.; Maramba, J.; Britt, M.; Scott, A. J.; Ernst, R. K.; Mihailescu, M.; Cotten, M. L.; Sukharev, S. Differential Interactions of Piscidins with Phospholipids and Lipopolysaccharides at Membrane Interfaces. *Langmuir* **2020**, *36*, 5065−5077.

(53) Comert, F.; Heinrich, F.; Chowdhury, A.; Schoeneck, M.; Darling, C.; Anderson, K. W.; Libardo, M. D. J.; Angeles-Boza, A. M.; Silin, V.; Cotten, M. L.; Mihailescu, M. Copper-binding anticancer peptides from the piscidin family: an expanded mechanism that encompasses physical and chemical bilayer disruption. *Sci. Rep.* **2021**, *11*, 12620.

(54) Salger, S. A.; Cassady, K. R.; Reading, B. J.; Noga, E. J. A Diverse Family of Host-Defense Peptides (Piscidins) Exhibit Specialized Anti-Bacterial and Anti-Protozoal Activities in Fishes. *PLoS One* **2016**, *11*, No. e0159423.

(55) Moulay, G.; Leborgne, C.; Mason, A. J.; Aisenbrey, C.; Kichler, A.; Bechinger, B. Histidine-rich designer peptides of the LAH4 family promote cell delivery of a multitude of cargo. *J. Pept. Sci.* **2017**, *23*, 320−328.

(56) Roelants, S. L.; Ciesielska, K.; De Maeseneire, S. L.; Moens, H.; Everaert, B.; Verweire, S.; Denon, Q.; Vanlerberghe, B.; Van Bogaert, I. N.; Van der Meeren, P.; Devreese, B.; Soetaert, W. Towards the industrialization of new biosurfactants: Biotechnological opportunities for the lactone esterase gene from Starmerella bombicola. *Biotechnol. Bioeng.* **2016**, *113*, 550−9.

(57) De Graeve, M.; De Maeseneire, S. L.; Roelants, S. L. K. W.; Soetaert, W. Starmerella bombicola, an industrially relevant, yet

fundamentally underexplored yeast. *FEMS Yeast Research* **2018**, *18*, No. foy072.

(58) Dierickx, S.; Castelein, M.; Remmery, J.; De Clercq, V.; Lodens, S.; Baccile, N.; De Maeseneire, S. L.; Roelants, S. L. K. W.; Soetaert, W. K. From bumblebee to bioeconomy: Recent developments and perspectives for sophorolipid biosynthesis. *Biotechnol. Adv.* **2022**, *54*, No. 107788.

(59) Morya, V. K.; Ahn, C.; Jeon, S.; Kim, E. K. Medicinal and cosmetic potentials of sophorolipids. *Mini Rev. Med. Chem.* **2013**, *13*, 1761−8.

(60) Fu, S. L.; Wallner, S. R.; Bowne, W. B.; Hagler, M. D.; Zenilman, M. E.; Gross, R.; Bluth, M. H. Sophorolipids and their derivatives are lethal against human pancreatic cancer cells. *J. Surg. Res.* **2008**, *148*, 77−82.

(61) Shah, V.; Doncel, G. F.; Seyoum, T.; Eaton, K. M.; Zalenskaya, I.; Hagver, R.; Azim, A.; Gross, R. Sophorolipids, microbial glycolipids with anti-human immunodeficiency virus and sperm-immobilizing activities. *Antimicrob. Agents Chemother.* **2005**, *49*, 4093−100.

(62) Koh, A.; Linhardt, R. J.; Gross, R. Effect of Sophorolipid n-Alkyl Ester Chain Length on Its Interfacial Properties at the Almond Oil−Water Interface. *Langmuir* **2016**, *32*, 5562−5572.

(63) Shao, L.; Song, X.; Ma, X.; Li, H.; Qu, Y. Bioactivities of Sophorolipid with Different Structures Against Human Esophageal Cancer Cells. *J. Surg Res.* **2012**, *173*, 286−291.

(64) Totsingan, F.; Liu, F.; Gross, R. A. Structure-Activity Relationship Assessment of Sophorolipid Ester Derivatives against Model Bacteria Strains. *Molecules* **2021**, *26*, 3021.

(65) Gao, R.; Falkeborg, M.; Xu, X.; Guo, Z. Production of sophorolipids with enhanced volumetric productivity by means of high cell density fermentation. *Appl. Microbiol. Biotechnol.* **2013**, *97*, 1103−11.

(66) Bisht, K. S.; Gross, R. A.; Kaplan, D. L. Enzyme-Mediated Regioselective Acylations of Sophorolipids. *J. Org. Chem.* **1999**, *64*, 780−789.

(67) Koh, A.; Todd, K.; Sherbourne, E.; Gross, R. A. Fundamental Characterization of the Micellar Self-Assembly of Sophorolipid Esters. *Langmuir* **2017**, *33*, 5760−5768.

(68) Koh, A.; Gross, R. Molecular editing of sophorolipids by esterification of lipid moieties: Effects on interfacial properties at paraffin and synthetic crude oil-water interfaces. *Colloids Surf. A: Physicochem* **2016**, *507*, 170−181.

(69) Ben Messaoud, G.; Promeneur, L.; Brennich, M.; Roelants, S. L. K. W.; Le Griel, P.; Baccile, N. Complex coacervation of natural sophorolipid bolaamphiphile micelles with cationic polyelectrolytes. *Green Chem.* **2018**, *20*, 3371−3385.

(70) Cho, W. Y.; Ng, J. F.; Yap, W. H.; Goh, B. H. Sophorolipids-Bio-Based Antimicrobial Formulating Agents for Applications in Food and Health. *Molecules* **2022**, *27*, 5556.

(71) Chekmenev, E. Y.; Jones, S. M.; Nikolayeva, Y. N.; Vollmar, B. S.; Wagner, T. J.; Gor'kov, P. L.; Brey, W. W.; Manion, M. N.; Daugherty, K. C.; Cotten, M. High-field NMR studies of molecular recognition and structure-function relationships in antimicrobial piscidins at the water-lipid bilayer interface. *J. Am. Chem. Soc.* **2006**, *128*, 5308−5309.

(72) Schwalbe, R.; Steele-Moore, L.; Goodwin, A. *Antimicrobial susceptibility testing protocols*; CRC Press: Boca Raton, 2007; p 432.

(73) Ayaz, M.; Ullah, F.; Sadiq, A.; Ullah, F.; Ovais, M.; Ahmed, J.; Devkota, H. P. Synergistic interactions of phytochemicals with antimicrobial agents: Potential strategy to counteract drug resistance. *Chem. Biol. Interact* **2019**, *308*, 294−303.

(74) Odds, F. C. Synergy, antagonism, and what the chequerboard puts between them. *J. Antimicrob. Chemother.* **2003**, *52*, 1.

(75) Ratledge, C.; Wilkinson, S. G. An overview of microbial lipids. In *Microbial Lipids*; Ratledge, C., Wilkinson, S. G., Eds.; Academic Press: London, 1988; Vol. *1*, pp 3−22.

(76) Chekmenev, E.; Vollmar, B.; Cotten, M. Can antimicrobial peptides scavenge around a cell in less than a second? *Biochim. Biophys. Acta* **2010**, *1798*, 228−234.

(77) Perrin, B. S., Jr; Tian, Y.; Fu, R.; Grant, C. V.; Chekmenev, E. Y.; Wieczorek, W. E.; Dao, A. E.; Hayden, R. M.; Burzynski, C. M.; Venable, R. M.; Sharma, M.; Opella, S. J.; Pastor, R. W.; Cotten, M. L. High-resolution structures and orientations of antimicrobial peptides piscidin 1 and piscidin 3 in fluid bilayers reveal tilting, kinking, and bilayer immersion. *J. Am. Chem. Soc.* **2014**, *136*, 3491−3504.

(78) Paredes, S. D.; Kim, S.; Rooney, M. T.; Greenwood, A. I.; Hristova, K.; Cotten, M. L. Enhancing the membrane activity of Piscidin 1 through peptide metallation and the presence of oxidized lipid species: Implications for the unification of host defense mechanisms at lipid membranes. *Biochim Biophys Acta Biomembr* **2020**, *1862*, No. 183236.

(79) Ramamoorthy, A.; Thennarasu, S.; Lee, D. K.; Tan, A.; Maloy, L. Solid-state NMR investigation of the membrane-disrupting mechanism of antimicrobial peptides MSI-78 and MSI-594 derived from magainin 2 and melittin. *Biophys. J.* **2006**, *91*, 206−216.

(80) Mason, A. J.; Marquette, A.; Bechinger, B. Zwitterionic phospholipids and sterols modulate antimicrobial peptide-induced membrane destabilization. *Biophys. J.* **2007**, *93*, 4289−4299.

(81) Sherman, P. J.; Jackway, R. J.; Gehman, J. D.; Praporski, S.; McCubbin, G. A.; Mechler, A.; Martin, L. L.; Separovic, F.; Bowie, J. H. Solution Structure and Membrane Interactions of the Antimicrobial Peptide Fallaxidin 4.1a: An NMR and QCM Study. *Biochemistry* **2009**, *48*, 11892−11901.

(82) Chen, P. S.; Toribara, T. Y.; Warner, H. Microdetermination of Phosphorus. *Anal. Chem.* **1956**, *28*, 1756−1758.

(83) Sani, M. A.; Gagne, E.; Gehman, J. D.; Whitwell, T. C.; Separovic, F. Dye-release assay for investigation of antimicrobial peptide activity in a competitive lipid environment. *Eur. Biophys J.* **2014**, *43*, 445−450.

(84) Hall, K.; Lee, T. H.; Mechler, A. I.; Swann, M. J.; Aguilar, M. I. Real-time measurement of membrane conformational states induced by antimicrobial peptides: balance between recovery and lysis. *Sci. Rep* **2014**, *4*, 5479.

(85) Wu, C. S.; Ikeda, K.; Yang, J. T. Ordered conformation of polypeptides and proteins in acidic dodecyl sulfate solution. *Biochemistry* **1981**, *20*, 566−70.

(86) Lee, S. A.; Kim, Y. K.; Lim, S. S.; Zhu, W. L.; Ko, H.; Shin, S. Y.; Hahm, K.; Kim, Y. Solution structure and cell selectivity of piscidin 1 and its analogues. *Biochemistry* **2007**, *46*, 3653−3663.

(87) Fu, R.; Gordon, E. D.; Hibbard, D. J.; Cotten, M. High resolution heteronuclear correlation NMR spectroscopy of an antimicrobial peptide in aligned lipid bilayers: Peptide−water interactions at the water−bilayer interface. *J. Am. Chem. Soc.* **2009**, *131*, 10830−10831.

(88) Hohwy, M.; Nielsen, N. C. Elimination of high order terms in multiple pulse nuclear magnetic resonance spectroscopy: Application to homonuclear decoupling in solids. *J. Chem. Phys.* **1997**, *106*, 7571−7586.

(89) Blaurock, A. E. Structure of the nerve myelin membrane: proof of the low-resolution profile. *J. Mol. Biol.* **1971**, *56*, 35−52.

(90) Franks, N. P.; Levine, Y. K. Low-angle x-ray diffraction. *Mol. Biol. Biochem Biophys* **1981**, *31*, 437−87.

(91) Matsuzaki, K.; Sugishita, K.-i.; Ishibe, N.; Ueha, M.; Nakata, S.; Miyajima, K.; Epand, R. M. Relationship of Membrane Curvature to the Formation of Pores by Magainin 2. *Biochemistry* **1998**, *37*, 11856−11863.

(92) Wang, J.; Mura, M.; Zhou, Y.; Pinna, M.; Zvelindovsky, A. V.; Dennison, S. R.; Phoenix, D. A. The cooperative behaviour of antimicrobial peptides in model membranes. *Biochim. Biophys. Acta* **2014**, *1838*, 2870−81.

(93) Meletiadis, J.; Pournaras, S.; Roilides, E.; Walsh, T. J. Defining fractional inhibitory concentration index cutoffs for additive interactions based on self-drug additive combinations, Monte Carlo simulation analysis, and in vitro-in vivo correlation data for antifungal drug combinations against Aspergillus fumigatus. *Antimicrob. Agents Chemother.* **2010**, *54*, 602−9.

(94) Brogden, K. A. Antimicrobial peptides: Pore formers or metabolic inhibitors in bacteria? *Nature Reviews Microbiology* **2005**, *3*, 238−250.

(95) Shai, Y. Mode of action of membrane active antimicrobial peptides. *Biopolymers (Peptide Science)* **2002**, *66*, 236−248.

(96) Guha, S.; Ghimire, J.; Wu, E.; Wimley, W. C. Mechanistic Landscape of Membrane-Permeabilizing Peptides. *Chem. Rev.* **2019**, *119*, 6040−6085.

(97) Wang, T.; Turko, I. V. Proteomic Toolbox To Standardize the Separation of Extracellular Vesicles and Lipoprotein Particles. *J. Proteome Res.* **2018**, *17*, 3104−3113.

(98) Wang, T.; Anderson, K. W.; Turko, I. V. Assessment of Extracellular Vesicles Purity Using Proteomic Standards. *Anal. Chem.* **2017**, *89*, 11070−11075.

(99) Lee, S. A.; Kim, Y. K.; Lim, S. S.; Zhu, W. L.; Ko, H.; Shin, S. Y.; Hahm, K. S.; Kim, Y. Solution structure and cell selectivity of piscidin 1 and its analogues. *Biochemistry* **2007**, *46*, 3653−3663.

(100) Barjat, H.; Morris, G. A.; Smart, S.; Swanson, A. G.; Williams, S. C. R. High-Resolution Diffusion-Ordered 2D Spectroscopy (HR-DOSY) - A New Tool for the Analysis of Complex Mixtures. *J. Magn Reson, Ser. B* **1995**, *108*, 170−172.

(101) Seelig, J.; Macdonald, P. M.; Scherer, P. G. Phospholipid head groups as sensors of electric charge in membranes. *Biochemistry* **1987**, *26*, 7535−41.

(102) Su, Y.; DeGrado, W. F.; Hong, M. Orientation, dynamics, and lipid interaction of an antimicrobial arylamide investigated by 19F and 31P solid-state NMR spectroscopy. *J. Am. Chem. Soc.* **2010**, *132*, 9197−205.

(103) Henzler-Wildman, K. A.; Lee, D. K.; Ramamoorthy, A. Mechanism of lipid bilayer disruption by the human antimicrobial peptide, LL-37. *Biochemistry* **2003**, *42*, 6545−6558.

(104) Bechinger, B.; Salnikov, E. S. The membrane interactions of antimicrobial peptides revealed by solid-state NMR spectroscopy. *Chem. Phys. Lipids* **2012**, *165*, 282−301.

(105) Ouellet, M.; Otis, F.; Voyer, N.; Auger, M. Biophysical studies of the interactions between 14-mer and 21-mer model amphipathic peptides and membranes: Insights on their modes of action. *Biochim Biophys Acta Biomembr* **2006**, *1758*, 1235−1244.

(106) Tremouilhac, P.; Strandberg, E.; Wadhwani, P.; Ulrich, A. S. Conditions affecting the re-alignment of the antimicrobial peptide PGLa in membranes as monitored by solid state ^{2}H-NMR. *Biochim. Biophys. Acta* **2006**, *1758*, 1330−42.

(107) Marcotte, I.; Wegener, K.; Lam, Y.; Chia, B.; de Planque, M.; Bowie, J.; Auger, M.; Separovic, F. Interaction of antimicrobial peptides from Australian amphibians with lipid membranes. *Chem. Phys. Lipids* **2003**, *122*, 107−20.

(108) Cross, T. A.; Opella, S. J. Solid-state NMR structural studies of peptides and proteins in membranes. *Curr. Opin Struct Biol.* **1994**, *4*, 574−581.

(109) Bechinger, B.; Gierasch, L. M.; Montal, M.; Zasloff, M.; Opella, S. J. Orientations of helical peptides in membrane bilayers by solid state NMR spectroscopy. *Solid State NMR* **1996**, *7*, 185−191.

(110) Fu, R.; Cross, T. A. Solid-state NMR investigation of protein and polypeptide structure. *Annu. Rev. Biophys. Biomol. Struct.* **1999**, *28*, 235−268.

(111) Opella, S. J.; Marassi, F. M. Structure determination of membrane proteins by NMR spectroscopy. *Chem. Rev.* **2004**, *104*, 3587−3606.

(112) Scherer, P. G.; Seelig, J. Electric charge effects on phospholipid headgroups. Phosphatidylcholine in mixtures with cationic and anionic amphiphiles. *Biochemistry* **1989**, *28*, 7720−8.

(113) Pott, T.; Maillet, J.-C.; Abad, C.; Campos, A.; Dufourcq, J.; Dufourc, E. J. The lipid charge density at the bilayer surface modulates the effects of melittin on membranes. *Chem. Phys. Lipids* **2001**, *109*, 209−223.

(114) Roux, M.; Beswick, V.; Coïc, Y.-M.; Huynh-Dinh, T.; Sanson, A.; Neumann, J.-M. PMP1 18−38, A Yeast Plasma Membrane Protein Fragment, Binds Phosphatidylserine from Bilayer Mixtures with Phosphatidylcholine: A 2H-NMR Study. *Biophys. J.* **2000**, *79*, 2624−2631.

(115) Marassi, F. M.; Macdonald, P. M. Response of the headgroup of phosphatidylglycerol to membrane surface charge as studied by deuterium and phosphorus-31 nuclear magnetic resonance. *Biochemistry* **1991**, *30*, 10558−10566.

(116) Wang, J.; Denny, J.; Tian, C.; Kim, S.; Mo, Y.; Kovacs, F.; Song, Z.; Nishimura, K.; Gan, Z.; Fu, R.; Quine, J. R.; Cross, T. A. Imaging membrane protein helical wheels. *J. Magn. Reson.* **2000**, *144*, 162−167.

(117) Marassi, F. M.; Opella, S. J. A solid-state NMR index of helical membrane protein structure and topology. *J. Magn. Reson.* **2000**, *144*, 150−155.

(118) Tian, Y.; Schwieters, C. D.; Opella, S. J.; Marassi, F. M. AssignFit: A program for simultaneous assignment and structure refinement from solid-state NMR spectra. *J. Magn. Reson.* **2012**, *214*, 42−50.

(119) Hristova, K.; Wimley, W. C.; Mishra, V. K.; Anantharamiah, G. M.; Segrest, J. P.; White, S. H. An amphipathic alpha-helix at a membrane interface: a structural study using a novel X-ray diffraction method. *J. Mol. Biol.* **1999**, *290*, 99−117.

(120) Drin, G.; Casella, J. F.; Gautier, R.; Boehmer, T.; Schwartz, T. U.; Antonny, B. A general amphipathic alpha-helical motif for sensing membrane curvature. *Nat. Struct Mol. Biol.* **2007**, *14*, 138−46.

(121) Bechinger, B. The SMART model: Soft Membranes Adapt and Respond, also Transiently, in the presence of antimicrobial peptides. *J. Pept Sci.* **2015**, *21*, 346−55.

(122) Wenk, M. R.; Alt, T.; Seelig, A.; Seelig, J. Octyl-beta-D-glucopyranoside partitioning into lipid bilayers: thermodynamics of binding and structural changes of the bilayer. *Biophys. J.* **1997**, *72*, 1719−31.

(123) Cheng, M. H.; Pan, C. Y.; Chen, N. F.; Yang, S. N.; Hsieh, S.; Wen, Z. H.; Chen, W. F.; Wang, J. W.; Lu, W. H.; Kuo, H. M. Piscidin-1 Induces Apoptosis via Mitochondrial Reactive Oxygen Species-Regulated Mitochondrial Dysfunction in Human Osteosarcoma Cells. *Sci. Rep.* **2020**, *10*, 5045.

(124) Diaz-Rodriguez, P.; Chen, H.; Erndt-Marino, J. D.; Liu, F.; Totsingan, F.; Gross, R. A.; Hahn, M. S. Impact of Select Sophorolipid Derivatives on Macrophage Polarization and Viability. *ACS Appl. Bio Mater.* **2019**, *2*, 601−612.

(125) Tamargo, J.; Le Heuzey, J.-Y.; Mabo, P. Narrow therapeutic index drugs: a clinical pharmacological consideration to flecainide. *Eur. J. Clin Pharmacol* **2015**, *71*, 549−567.

(126) Campagna, S.; Saint, N.; Molle, G.; Aumelas, A. Structure and mechanism of action of the antimicrobial peptide piscidin. *Biochemistry* **2007**, *46*, 1771−1778.

(127) Cullis, P. R.; de Kruijff, B. Lipid polymorphism and the functional roles of lipids in biological membranes. *Biochim. Biophys. Acta* **1979**, *559*, 399−420.

(128) Seelig, J. ^{31}P nuclear magnetic resonance and the head group structure of phospholipids in membranes. *Biochim. Biophys. Acta* **1978**, *515*, 105−140.

(129) Filippov, A. V.; Khakimov, A. M.; Munavirov, B. V. Chapter Two - 31P NMR Studies of Phospholipids. In *Annual Reports on NMR Spectroscopy*; Webb, G. A., Ed.; Academic Press, 2015; Vol. 85, pp 27−92.

(130) Schiller, J.; Muller, M.; Fuchs, B.; Arnold, K.; Huster, D. 31P NMR Spectroscopy of Phospholipids: From Micelles to Membranes. *Cur. Anal. Chem.* **2007**, *3*, 283−301.

(131) Grélard, A.; Loudet, C.; Diller, A.; Dufourc, E. J. NMR spectroscopy of lipid bilayers. *Methods Mol. Biol. (Clifton, NJ)* **2010**, *654*, 341−359.

(132) Szlasa, W.; Zendran, I.; Zalesińska, A.; Tarek, M.; Kulbacka, J. Lipid composition of the cancer cell membrane. *J. Bioenerg Biomembr* **2020**, *52*, 321−342.

(133) Lin, H.-J.; Huang, T.-C.; Muthusamy, S.; Lee, J.-F.; Duann, Y.-F.; Lin, C.-H. Piscidin-1, an Antimicrobial Peptide from Fish (Hybrid Striped Bass Morone saxatilis x M. chrysops), Induces Apoptotic and Necrotic Activity in HT1080 Cells. *Zoolog. Sci.* **2012**, *29*, 327−332.

(134) Elshikh, M.; Moya-Ramírez, I.; Moens, H.; Roelants, S.; Soetaert, W.; Marchant, R.; Banat, I. M. Rhamnolipids and lactonic sophorolipids: natural antimicrobial surfactants for oral hygiene. *J. Appl. Microbiol.* **2017**, *123*, 1111−1123.

(135) Thakur, P.; Saini, N. K.; Thakur, V. K.; Gupta, V. K.; Saini, R. V.; Saini, A. K. Rhamnolipid the Glycolipid Biosurfactant: Emerging trends

and promising strategies in the field of biotechnology and biomedicine. *Microb. Cell Fact.* **2021**, *20*, 1.

(136) Abalos, A.; Pinazo, A.; Infante, M. R.; Casals, M.; García, F.; Manresa, A. Physicochemical and Antimicrobial Properties of New Rhamnolipids Produced by Pseudomonas aeruginosa AT10 from Soybean Oil Refinery Wastes. *Langmuir* **2001**, *17*, 1367−1371.

(137) Ortiz, A.; Teruel, J. A.; Espuny, M. J.; Marqués, A.; Manresa, A.; Aranda, F. J. Effects of dirhamnolipid on the structural properties of phosphatidylcholine membranes. *Int. J. Pharm.* **2006**, *325*, 99−107.

(138) Sana, S.; Datta, S.; Biswas, D.; Sengupta, D. Assessment of synergistic antibacterial activity of combined biosurfactants revealed by bacterial cell envelop damage. *Biochim Biophys Acta Biomembr* **2018**, *1860*, 579−585.

(139) Magalhães, L.; Nitschke, M. Antimicrobial activity of rhamnolipids against Listeria monocytogenes and their synergistic interaction with nisin. *Food Control* **2013**, *29*, 138−142.

(140) Fu, R.; Rooney, M. T.; Zhang, R.; Cotten, M. L. Coordination of Redox Ions within a Membrane-Binding Peptide: A Tale of Aromatic Rings. *J. Phys. Chem. Lett.* **2021**, *12*, 4392−4399.

(141) Rai, R. K.; De Angelis, A.; Greenwood, A.; Opella, S. J.; Cotten, M. L. Metal-ion Binding to Host Defense Peptide Piscidin 3 Observed in Phospholipid Bilayers by Magic Angle Spinning Solid-state NMR. *ChemPhysChem* **2019**, *20*, 295.

(142) Strandberg, E.; Zerweck, J.; Wadhwani, P.; Ulrich, A. S. Synergistic insertion of antimicrobial magainin-family peptides in membranes depends on the lipid spontaneous curvature. *Biophys. J.* **2013**, *104*, L9−11.

(143) Aisenbrey, C.; Amaro, M.; Pospíšil, P.; Hof, M.; Bechinger, B. Highly synergistic antimicrobial activity of magainin 2 and PGLa peptides is rooted in the formation of supramolecular complexes with lipids. *Sci. Rep* **2020**, *10*, 11652.